

Chronological Evolution of Stability in Hybrid Halide Perovskite Solar Cells

Parvesh K. Deendyal, Shweta Dhakla, Ankur Taya, Renu Singla, Harpreet Singh, Sarvesh Kumar, Timothy A. Hackett, Manish K. Kashyap,* Dania Ali, and Ali H. Reshak*

Hybrid halide perovskite (HHP) emerged as an excellent material for upcoming photovoltaic technologies owing to its rapid performance growth just within a decade. Extensive research worldwide is going on HHP due to their unique optical properties, flexible thin-film nature, and simple low-cost solution-based fabrication processes for solar cells. Albeit HHP solar cells exhibit adequate power conversion efficiency (PCE), poor stability impedes its commercial deployment. This review summarizes the major efforts made worldwide to improve the stability of HHP-based solar cells from time to time. Methyl ammonium lead halide (MAPbI₃) has been first used in HHP-based perovskite solar cells (PSCs) but it is more vulnerable to heat and moisture. Further, formamidinium (FA⁺) and guanidinium (GA⁺) ion doping have been adopted as a compositional modification for better structural and environmental stability. The entire work has been categorized into three sub-areas, i.e., MA, FA, and GA-based HHP solar cells and the comparison of various photovoltaic parameters of these cells has been presented. Furthermore, the challenges and prospects for PSC research and development toward commercialization have also been presented.

1. Introduction

Over the past decade, hybrid halide perovskite solar cells (PSCs) have witnessed the most significant advances in the field of photovoltaics. The rapid progress observed in the performance of emerging thin-film PSC technology is unprecedented. Perovskites are optically active semiconducting materials with exceptional optoelectronic and chemical properties. In 1839, a Russian mineralogist Gustav Rose discovered the first perovskite material CaTiO₃ and named it in honor of another renowned Russian mineralogist Lev A. Perovski.^[1] Afterward, a number of inorganic metal oxides were found to have a similar structure to that of perovskite, e.g., PbTiO₃, BaTiO₃, BiFeO₃, etc. Therefore, all the materials having similar composition and structure to CaTiO₃ were


P. K. Deendyal, S. Dhakla, M. K. Kashyap
Renewable Energy Laboratory
School of Physical Sciences
Jawaharlal Nehru University
New Delhi 110067, India
E-mail: mkkashyap@mail.jnu.ac.in

P. K. Deendyal
Department of Applied Science
Government Polytechnic for Women
Faridabad 121006, Haryana, India

A. Taya
Department of Physics
Mukand Lal National College
Yamunanagar, Haryana 135001, India

R. Singla
Department of Physics
Daulat Ram College, University of Delhi
Delhi 110007, India

H. Singh
Department of Physics
IIHS
Kurukshetra University
Kurukshetra, Haryana 136119, India

 The ORCID identification number(s) for the author(s) of this article can be found under <https://doi.org/10.1002/solr.202300957>.

DOI: 10.1002/solr.202300957

S. Kumar
Inter-University Accelerator Centre (IUAC)
Aruna Asaf Ali Marg, New Delhi 110067, India

T. A. Hackett
Department of Biochemistry
University of Nebraska-Lincoln
Lincoln, NE68588-0664USA

D. Ali
Faculty of Medicine
Charles University
Pilsen 30100, Czech Republic

A. H. Reshak
Physics Department
College of Science
University of Basrah
Basrah, Iraq
E-mail: ali.reshak@uobasrah.edu.iq

A. H. Reshak
Al-Kunooz University College
Basrah, Iraq

A. H. Reshak
Center of Excellence Geopolymer and Green Technology
School of Material Engineering
University Malaysia Perlis
Kangar, Perlis 01007, Malaysia

named as perovskites.^[2] Hybrid halide perovskite (HHP) has a structure similar to CaTiO_3 with the generic chemical formula ABX_3 , where A and B are cations, X being an oxide or halide ion as illustrated in **Figure 1**. In all-inorganic halide perovskite suitable for photovoltaics, A^+ is Cs^+ or Rb^+ ,^[3,4] whereas, in HHP, Cs^+ is replaced fully or partially by an organic cation, e.g., CH_3NH_3^+ (methyl-ammonium, MA), $\text{NH}_2\text{CH}_2\text{NH}_2^+$ (formamidinium, FA) etc., B is a divalent metal cation (Pb^{2+} or Sn^{2+}), and X is a monovalent halide anion (I^- , Br^- , or Cl^-).^[5–7] The term hybrid refers to the presence of both organic and inorganic components. Herein, cation A^+ is located in a cubo-octahedra cavity formed by eight $[\text{BX}_6]^-$, while cation B is in 6-fold coordination with the halide ion.

Over the period of time, perovskites have aroused the interest of material scientists due to their abundance and diversity in behavior. Due to their peculiar properties, perovskites have significant potential in various applications other than photovoltaics (PV) such as light-emitting diodes, photodetectors, X-ray detectors, memory devices, and so on.^[8] Owing to this fact, halide perovskites have prompted a lot of multidisciplinary research all over the world, which demands knowledge of physics, chemistry, optics, and electronics. Precisely, the perovskite materials have extensive applications in PV technology due to their excellent optical and chemical properties, e.g., large absorption coefficient,^[9] high charge-carrier diffusion length,^[10] low trap density,^[11] and small exciton binding energy.^[12] One of the most important materials in this domain is methyl-ammonium lead iodide (MAPbI_3), which can absorb a wider spectrum of light compared to silicon.^[13]

Although perovskite materials were discovered more than a decade ago, but they jumped into PV industry only in 2009, when Miyaska et al.^[14] first employed MAPbI_3 and MAPbBr_3 as photoactive layers in the quantum dots and achieved power conversion efficiency (PCE) of 3.8% and 3.1%, respectively. It was a

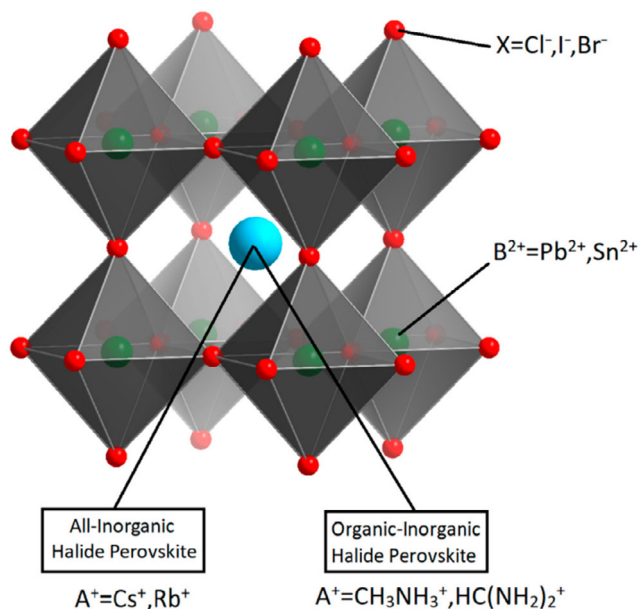


Figure 1. Systematic representation of the perovskite crystal with ABX_3 type structure.^[147]

delightful encounter with perovskite materials as it uncovered a new domain of PV, being a miraculous box with a plethora of enigmatic features. But, due to the device instability caused by a liquid electrolyte, this novel type of solar cell did not draw much attention at the time. In 2012, Lee et al.^[15] achieved a 10.9% efficiency by coating mixed halide perovskite ($\text{CH}_3\text{NH}_3\text{PbI}_{3-x}\text{Cl}_x$) over a compact layer of Al_2O_3 and deployed 2,2',7,7'-tetrakis(*n,n*-di-*p*-methoxyphenylamine)-9,9'-spirobifluorene (spiro-MeOTAD) as a solid-state organic hole transport layer (HTL). Since then, extensive research efforts have been put in by scientists worldwide which resulted in the unprecedented improvement in PCE from 3.8%^[14] to the recent value of 26.1%,^[16] which is already at par with the commercially available silicon solar cells.

In terms of practical applications, the development of PSCs has centered on two key challenges, one is PCE and another is long-term stability. Despite the tremendous progress in PCE, the state-of-the-art PSCs are still confined to the laboratories by virtue of due to low stability and less scalability.^[17] Perovskite degradation, due to external and internal factors, imposes the major bottleneck for commercialization. Indeed, over the past few years, the quest for long-term stability has become a hot research topic in PSCs, as a result, there is a drastic increment in the number of publications, from just 1 in 2012 to 2840 in the year 2022 as illustrated in **Figure 2**. It is noteworthy that understanding the degradation mechanisms caused by various degradation factors is crucial for the fabrication of more efficient and highly stable PSCs. According to several studies, both intrinsic and extrinsic factors such as light, heat, moisture, and oxygen are the major factors for performance deterioration. However, several encapsulation approaches have been developed to eliminate these external degradation causes.^[18,19] Encapsulated PSCs, in contrast, degrade rapidly under illumination due to their intrinsic degradation factors such as charge trapping and ion migration.

Commercially accessible silicon solar cells have great efficiency and stability, but the manufacturing process is tedious

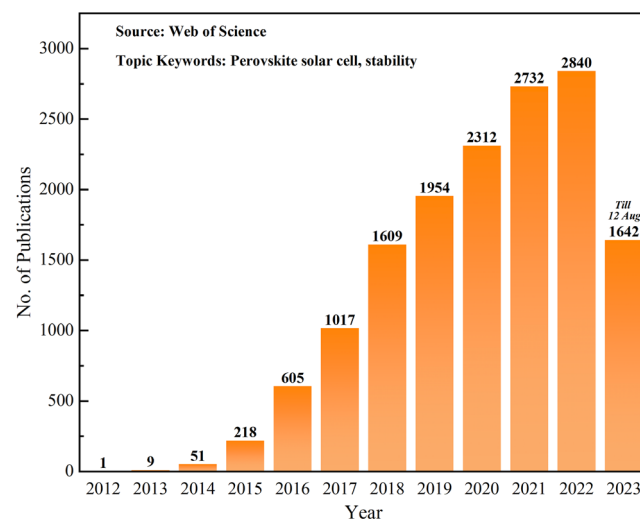


Figure 2. Annual progress of stability of PSCs with the increasing number of publications each year since 2012 (Source: Web of Science).

and expensive. Although dye-sensitized solar cells (DSSCs) are also available in the market, yet their efficiencies are still less than 15%.^[20] The PSCs, in contrast, are cost-effective, lightweight, and flexible. Along with the inexpensive solution-based fabrication process, perovskites have a remarkably high defect tolerant capacity, and suppressed carrier recombination.^[21] Therefore, among all the PV technologies of the twenty-first century, the PSCs offer a spark of hope for the advancement of renewable energy sources in terms of solar cells owing to their unique morphological and optoelectronic properties. Furthermore, the tunable bandgap of perovskites allows them to synergize with well-established silicon technology, pushing PCE beyond the theoretical limit of single junction cells. Recent advancements in the realm of perovskite/Si tandem devices have demonstrated efficiencies exceeding 30%,^[22] paving the way for next generation solar energy technologies. Nevertheless, to be marketable within the industry like Si PV panels, the PSCs must guarantee to yield stable power for a period of ≈ 25 years in outdoor conditions. The stability test for PSCs without encapsulation must be >500 h under 1 sun illumination and 1000 h under full sunlight.^[23,24] Scaling up PSCs from lab-scale to commercially viable modules always remains a hurdle. However, the researchers are continually attempting to address this challenge by optimizing techniques and materials for large-area fabrication.^[25,26] Overcoming these challenges will bring cost-effective, high-performance perovskite solar technology to the wider market.

Herein, the present review article mainly focuses on some fundamentals of PSCs and the various solution-based fabrication processes with a brief emphasis on the theoretical approach using important simulation software. It aims to analyze the chronological research evolution of stability in MA, FA, and guanidinium (GA)-based PSCs, emphasizing both inert and open environment conditions. Also, the future challenges

and expected solutions in the area of HHP-based solar cells are planned to outline. It ought to motivate the researchers to seek out and tackle multidisciplinary research issues with PSCs at present.

2. Synthesis of PSCs

The typical architecture of a PSC device mainly consists of indium tin oxide (ITO)/fluorine-doped tin oxide (FTO), electron transport layer (ETL), perovskite absorber layer, HTL, and the metal electrodes commonly called planar *n-i-p* type structure.^[27] In addition, there are a few more varieties of PSC architectures based on structural configurations, which are further divided into planar and mesoporous categories. Further, these different varieties of PSCs structure modules are shown in **Figure 3**.^[8] The perovskite layer is the most essential layer in the PSC device stack, therefore defect-free films with large grain size, crystal phase purity, and excellent film coverage are required to provide improved photovoltaic performance and stability. The efforts are being made to scale up the PV technology with a number of aspects being used for large-area PSCs' production, including both solution-based and vacuum deposition approaches. Device performance is highly influenced by a variety of parameters such as device architecture, compositional engineering, and film production process.^[28–31] Importantly, PSC's efficiency is generally dependent on the materials utilized in the various layers as well as the film deposition technique employed.^[32–36] The description of some important techniques for the thin film deposition of PSCs such as solutions-based processing methods like spin coating and dip coating, and roll-to-roll printing methods, with a focus on the parameters affecting the quality and the thickness of the coated thin films on the substrate are as follows:

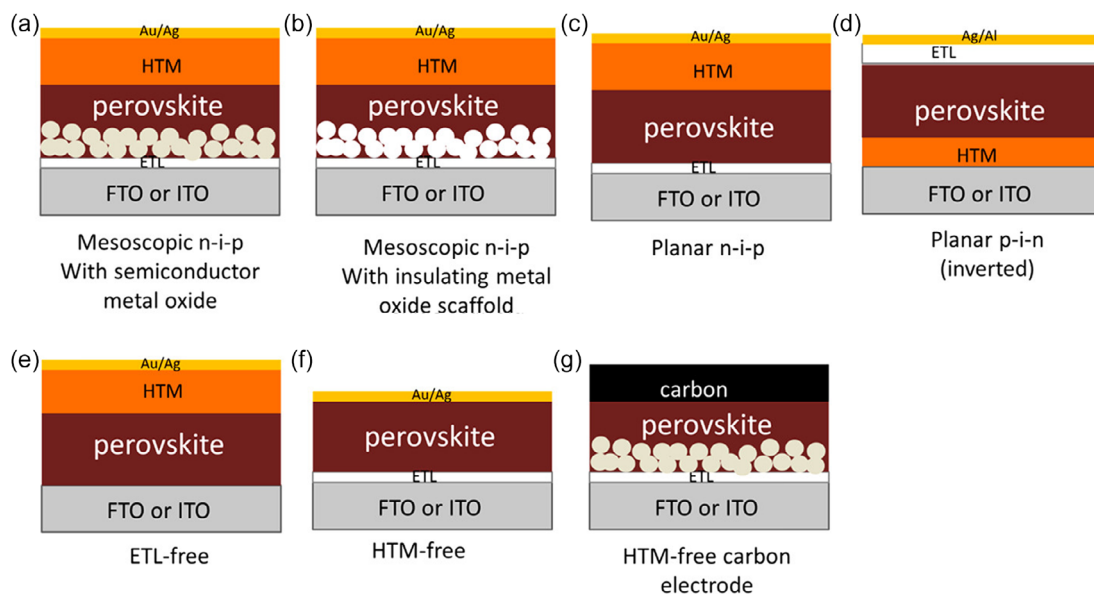


Figure 3. Various device architectures of PSCs a) mesoscopic *n-i-p* with semiconductor metal oxide, b) mesoscopic *n-i-p* with insulating metal oxide scaffold, c) planar *n-i-p*, d) planar *p-i-n* (inverted), e) ETL-free, f) HTM-free, and g) HTM-free carbon electrode.^[8]

2.1. Spin Coating

Spin coating is a facile and widely used technique for depositing thin film on rotating flat substrates by centrifugal forces.^[37] This method is mostly used for the fabrication of small area PSCs in laboratories. The growth of thin film by spin coating can be done in two ways. For the deposition of the MAPbI₃ perovskite absorbing layer in one step spin coating method, PbI₂ and CH₃NH₃I (MAI) are first dissolved together in dimethylformamide (DMF) or dimethyl sulfide (DMSO) solvent and mixed well to make a precursor solution. Then it is spin-coated on the ETL substrate to form a thin film of the photoactive layer. Whereas, in the two-step spin coating process, PbI₂ is deposited first individually and then MAI film as shown in **Figure 4a**.^[38] Further, the substrate is heated at a particular temperature after spin coating to produce a well-crystallized layer of perovskite. The quality and thickness of the thin film can be customized by adjusting the spin coating duration, acceleration, and spin speed. The film quality and properties are also affected by the annealing temperature and annealing time. Jiang et al.^[39] achieved 20.1% PCE on 1 cm² PSCs by using a two-step spin coating process. They fixed the spin coating speed for PbI₂ as 1500 rpm and varied for the upper CH(NH₂)₂I (FAI) layer as 1000, 1300, 1500, and 1700 rpm. The scanning electron microscope (SEM) image of various PBI₂/FAI combination layers is shown in **Figure 4b**. Albeit the efficiency achieved with the spin coating technique is quite good, this technique has demerits in large-scale production. The quality and homogeneity of the deposited film reduced sharply with an increase in the area.^[40] In the context of large substrates,

the film thickness varies from the center to the edge of the substrate.^[41,42]

2.2. Dip Coating

In the dip coating method, the substrate is first immersed in the aqueous solution of desired coating material. A uniform wet film is formed on the substrate's surface after its withdrawal from the solution at a regulated rate. The deposition of thin film by the dip coating method is depicted in **Figure 5i**.^[43] Further, the solvent can be evaporated by heating the substrate resulting in a coated thin film. The uniformity and thickness of the film depend on the withdrawal rate, solution concentration, number of dips, angle of dip, and drying angle. Huang et al.^[44] fabricated the TiO₂ film (ETL) and MAPbI₃ Perovskite film by the dip coating method and observed almost equal efficiency with the referenced spin-coated module. In addition, plane SEM images of both the spin and dip-coated perovskite films are shown in **Figure 5ii** along with the comparison between their absorbance and X-ray diffraction (XRD) pattern.

2.3. Roll-to-Roll Printing

The roll-to-roll (R2R) printing technology has already been envisioned as a way of ensuring large-scale PSCs commercialization, and this technique has been followed by extensive efforts in developing, refining, and augmenting laboratory-scale processes. This technique incorporates various coating methods which are

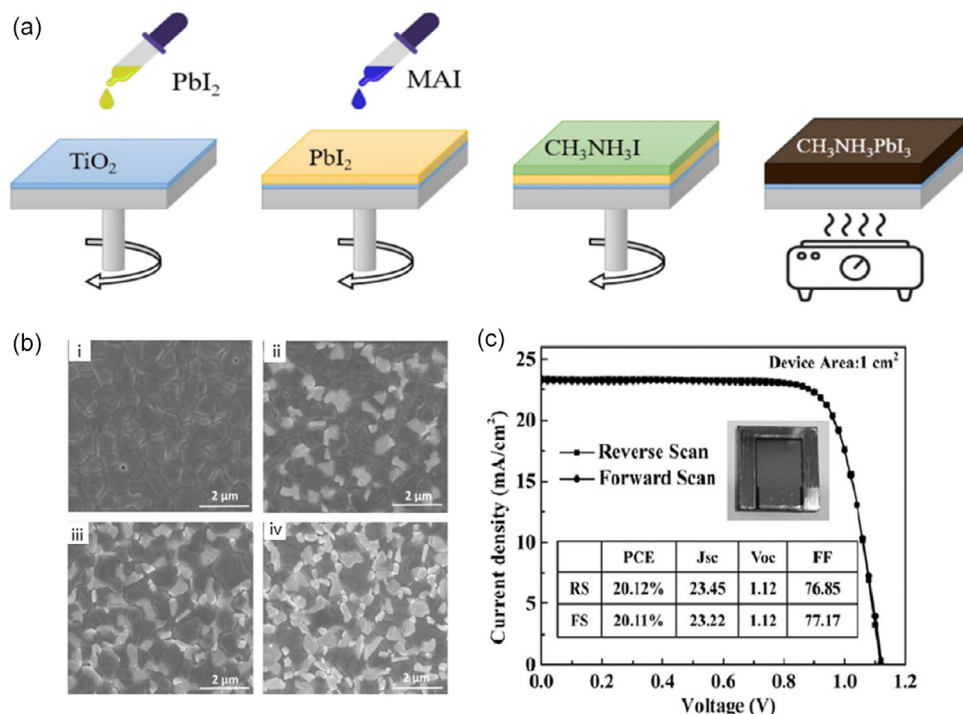


Figure 4. a) Two-step spin coating method for the deposition of MAPbI₃ perovskite on TiO₂ substrate. b) SEM images of perovskite layer with various PbI₂/FAI combinations, (i) Sample A with (1500/1000 rpm), (ii) Sample B (1500/1300 rpm), (iii) Sample C (1500/1500 rpm), (iv) Sample D (1500/1700 rpm); (scale bar: 2 μm)^[35] c) J–V characteristics of the best performing device in large size (1 cm²) in both reverse and forward scan; large area device and corresponding photovoltaic parameters are shown in the inset of **Figure (c)**.^[39]

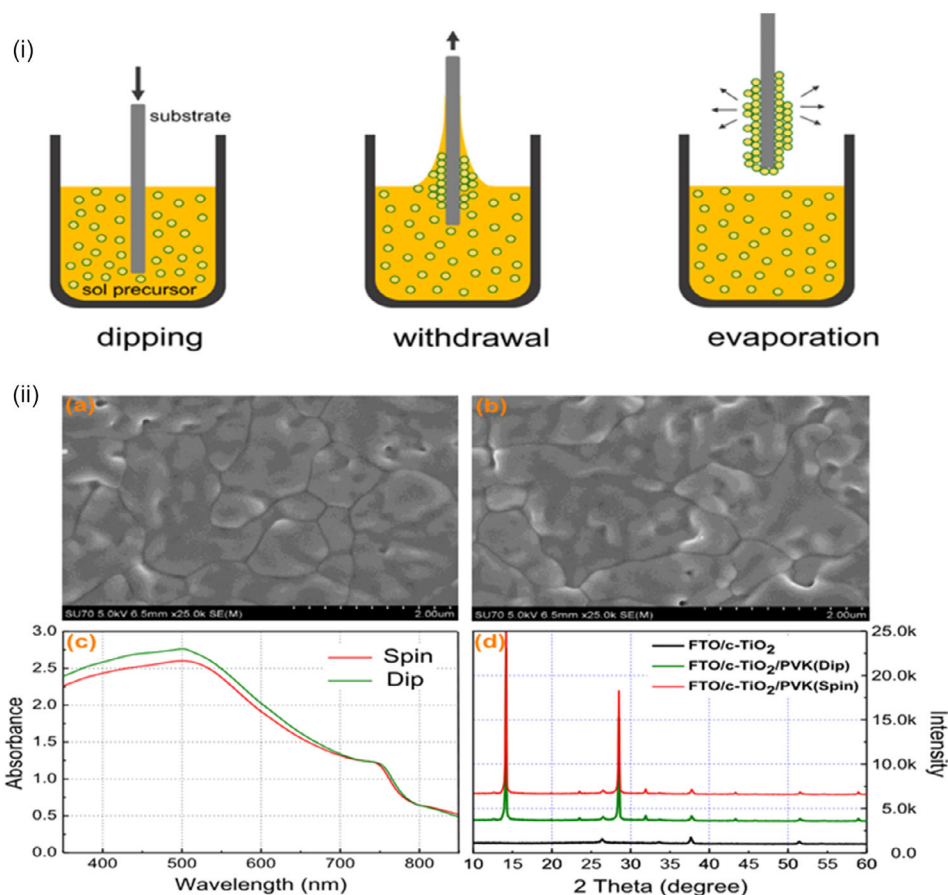


Figure 5. i) Sequential step for thin film deposition by dip coating method,^[43] ii) SEM images of the a) spin-coated, b) dip-coated perovskite films, c) UV-Vis absorption spectra, and d) XRD patterns of the dip-coated and spin-coated perovskite films.^[44]

used to print different layers of PSCs by using rotating rolls. In R2R printing, ETL precursor, perovskite precursor, and HTL can be coated in a sequence as illustrated in **Figure 6**.^[45] Due to the flow line production, the process is fast and cost-effective relative to spin and dip coating and presents a rich probability of high throughput fabrication of flexible solar cells.^[46–49] The several techniques which are compatible with R2R printing are spray coating, slot die coating, blade coating, ink-jet printing, gravure printing, and flexographic printing. Among all these, slot die coating is the most desirable method due to low precursor consumption and supreme layer thickness uniformity.^[50]

2.4. Thermal Evaporation Technique

In the previous section, it has been alluded that there are various deposition methods for fabricating the thin films of HTL, ETL, and the absorber layer of PSCs. While for their functioning as the solar cells, metal contacts should be prepared above the p-n junction which can be done with the help of a thermal evaporator.

Thermal evaporation is a high-vacuum technique for fabricating thin films of different materials on the substrate. Due to its ease of use, high deposition rate, and low equipment cost, thermal evaporation is a trendy physical vapor deposition technique.

The thickness of the films is typically in the range of a few angstroms (Å) to several hundred nanometers (nm). The method entails heating a solid source material until it reaches a particular vapor pressure. Thereafter, the evaporated material reaches the substrate and adheres to it, forming the necessary coating layer. A complete setup of a thermal evaporator and an illustration of thin film deposition by this method is shown in **Figure 7**.^[51,52] For two reasons, when gas is evacuated from a chamber, vapor molecules inside it can travel longer distances before colliding with a gas molecule. During evaporation, collisions with gas molecules are undesired because they shift the direction of travel of the substance vapor, affecting the substrate coverage. Second, for film purity, a high vacuum is essential. Contamination of the growing film is possible due to background gases in the chamber. This process may deposit a wide range of materials, including aluminum, silver, nickel, chrome, magnesium, and many others.

2.5. Theoretical Approach: Simulation and Analysis of PSCs

So far, we have discussed the experimental part of the PSCs module. In the context of the theoretical approach, various first-principles techniques can be used to predict the desired properties of materials. The density functional theory (DFT) is

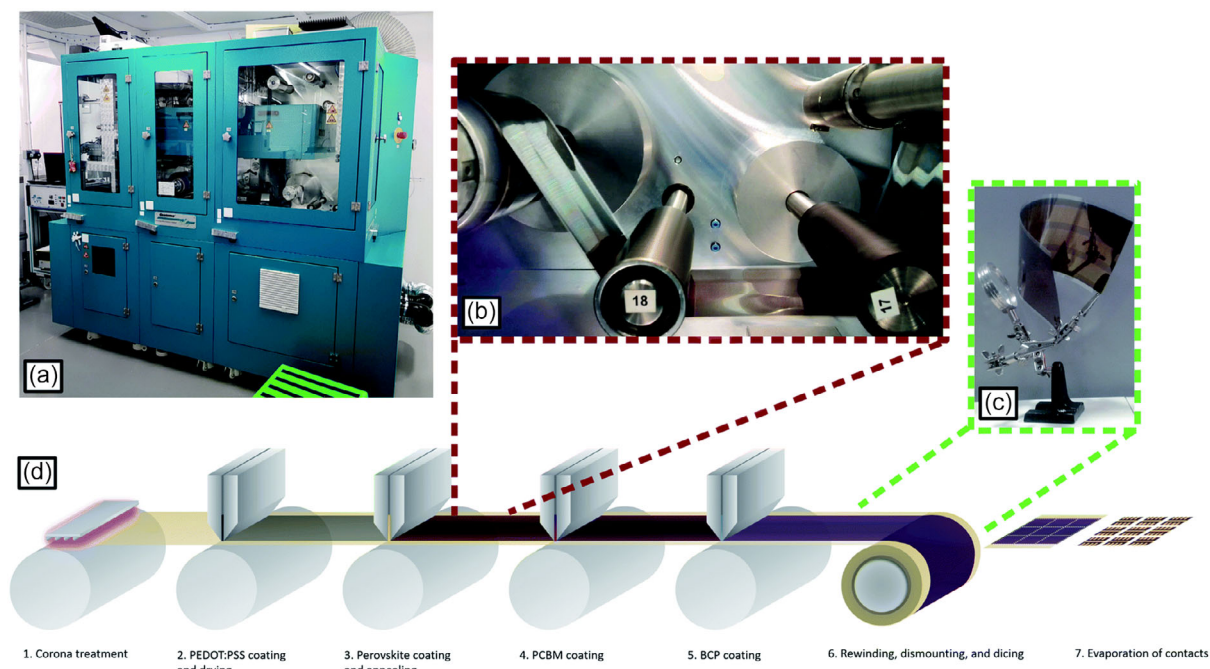


Figure 6. a) Smartcoater SC08 for R2R printing, b) R2R coated perovskite film, c) roll-to-roll coated flexible substrate having four slot-die deposited layers, and d) schematic diagram of a fully inline coating process with R2R slot-die coating process.^[45]

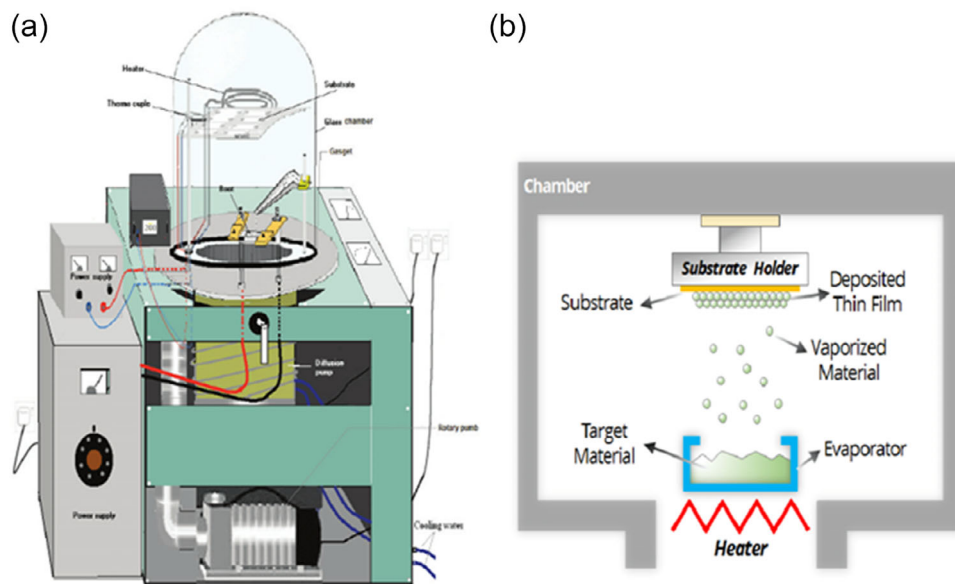


Figure 7. a) Complete set-up of a thermal evaporator. Reproduced with permission.^[51] Copyright 2012, Springer Nature. b) a schematic diagram of thin film deposition by thermal evaporation technique.^[52] Copyright 2012, Springer Nature.

the most preferable modeling method as it provides a good level of accuracy in the results.^[53–56] DFT is a quantum mechanical approach that can be used to accurately analyze the ground state and excited state properties of computationally synthesized materials. In other words, the *ab-initio* DFT technique can be used to examine the structural, optical, magnetic, and electronic aspects of many-body systems using a potential acting on the system's

electrons. This DFT potential incorporates an external potential V_{ext} , determined by the elemental composition of the system and its structure, and an effective potential V_{eff} , due to the interelectronic interactions.

Apart from DFT, various other theoretical approaches can also be employed to explore and analyze the domain of PSCs. These alternate approaches complement DFT-based simulations and

give a unique insight into the PSCs. One such more sophisticated approach is many body perturbation theory (MBPT) that inculcates the very crucial electron–electron interactions and provides a better insight into the understanding of excited state properties and evaluates accurate optical spectra and carrier lifetimes of charge carriers in PSCs.^[57] The typically used approximation in MBPT is GW approximation which gives correct predictions about electronic structures and optical properties by taking into account the self-energy corrections to electronic band structures.^[58]

DFT is mainly concerned about predicting the ground state electronic properties of perovskites but to understand and predict the dynamical behavior of electrons, atoms, and molecules in HHPs, one needs to go beyond DFT. In such scenarios, time dependent density functional theory (TD-DFT) comes handy.^[59] The quantum mechanical framework of TD-DFT plays a very pivotal role in understanding the dynamics that goes behind the interaction of light with the different layers of PSCs. The exchange-correlation functionals in TD-DFT relies not only on the spatial density of electrons but also on their time dependent density.

Quantum Monte Carlo (QMC), though a non-perturbative approach, is also well suited to study the perovskite materials owing to their multiple interaction components like electrons, holes, and defects.^[60] Alongside ground and excited state properties, this quantum mechanical approach also allows us to model and predict transport properties and recombination rates of various charge carriers in PSCs, thus providing a very valuable insight for optimizing the PCE. Apart from that, QMC is a great tool to study the defect dynamics and their interaction with charge carriers in PSC, which can be significantly advantageous in identifying and mitigating the effect of detrimental defects by developing strategies for enhancing the stability and performance of PSCs.

Being a computational method that combines the principles of quantum mechanics with molecular dynamics, *ab-initio* molecular dynamics (AIMD) is a potent tool for understanding the atomic scale dynamics in PSCs.^[61] This method is applied to simulate the growth of perovskite films from vapors or solutions, revealing information about the factors that govern the high-quality film formation in these solar cells. AIMD can give a comprehensive analysis of the effect of temperature, pressure, and moisture on the diversified categories of absorber, ETL, and HTLs of PSCs and the ion-migrations and material degradation thereafter, thus vital in understanding the performance and durability of PSCs in real world operating conditions. Moreover, by simulating different perovskite structures and compositions, AIMD can aid in the designing and optimization of more efficient and stable perovskite materials for PSCs.

In conjunction with the above approaches, semi-empirical models also found usefulness in the deliberations on the development of PSCs.^[62,63] These models join both empirical and theoretical approaches to describe the perovskite materials and predict their performance in PSCs. Insights into the stability, charge transport, and optoelectronic properties can be conferred alongside material screening for promising candidates and interface engineering for optimized charge extraction and reduced combinations at different interfaces of PSCs.

Above all these approaches, more recently machine learning (ML) and data driven approaches have captured the attention of materials scientists owing to their potential to revolutionize the way materials are discovered.^[64,65] Due to the accumulation and availability of a large amount of experimentally and theoretically obtained data on perovskite materials' structure, properties, and behavior, ML offered various innovative ways to understand, optimize, and accelerate the development of PSCs. The materials informatics are being used to develop models, databases, and algorithms to enable data-driven perovskites discovery and designing. The ability of ML models to predict properties of the perovskite materials based on compositional and structural features facilitates the identification of desired perovskite for solar cell applications. The algorithms utilized in various ML models can quickly screen and prioritize the tailored perovskite materials with promising properties, considerably diminishing the resources and time required for experimental synthesizing and testing, highlighting that ML has become an indispensable tool for PSCs material discovery and designing.

Numerical simulation is a significant and vital tool for predicting solar cell performance and providing practical direction for optimizing different geometrical and technical aspects of solar cells.^[66–71] The simulation can demonstrate the physical action, and the feasibility of a specified physical model, and is a useful way to examine how device parameters impact the physical operation and device performance without having to wait long. Throughout the field of photovoltaics, numerous simulation models are being used like AMPS, COMSOL MULTIPHYSICS, GPVDM, SCAPS-1D, SETFOS, SILVACO, and TCAD. One of the most commonly adopted device simulators for PSCs is SCAPS-1D. Solar Cell Capacitance Simulator (SCAPS-1D) is one-dimensional simulation software, developed at the Department of Electronics and Information Systems (ELIS), University of Gent, for analyzing the performance of thin film solar cells. The three primary differential equations which are used in the simulator are Poisson's equation, transport equation, and continuity equation.^[72]

Nishat et al.^[73] calculated the carrier mobility, absorption spectrum, and band gap of ETL layer TiO₂ using DFT. Further, the performance of a PSC was evaluated using the extracted properties in the SCAPS-1D device simulator. Also, Laali et al.^[74] calculated the absorption spectrum of MAPbI₃ and MAPbBr₃ perovskite layer and ZnO ETL layer by the DFT method and employed the results in the SCAPS-1D simulator. SETFOS, by Fluxim, is another major simulation programme for the analysis of organic photovoltaics (OPV) and organic light emitting diodes (OLEDs). Lekshmi et al.^[75] studied the performance of inverted PSCs for different HTLs by using SETFOS simulations.

3. Characterization

It is very important to produce stable perovskite thin film for effective use in the complete solar cell. Thus, it is important to perform a systematic analysis of the perovskite thin film separately. The following section is dedicated to the characterization of perovskite thin films first and then the complete perovskite solar cells.

3.1. Perovskite Thin Films

Perovskite thin films, at the forefront of cutting-edge optoelectronic applications, undergo meticulous characterizations employing a comprehensive methodology that integrates several techniques to unveil their structural, compositional, and morphological attributes, etc. The structural characterization is commonly accomplished by XRD, a powerful tool that offers insights into the phase purity, crystallographic orientation, and lattice parameters of the perovskite films. Further, this method enables the researchers to confirm the idealized ABX_3 perovskite structure and explore any possible deviations or imperfections in the material. For a better understanding of the film quality and surface properties, it is imperative to conduct the morphological investigations of perovskite films. In this regard, the techniques such as atomic force microscopy (AFM) and SEM are commonly used to visualize the grain size, topography, and surface roughness of the perovskite thin films. These findings are crucial owing to their direct influence on the charge transport properties and the overall performance of perovskite based PV devices.^[76] Furthermore, the analysis of perovskite film's composition involves a detailed examination of its chemical constituents, addressing aspects such as presence of defects, dopants, and additives. X-ray photoelectron spectroscopy (XPS) is a popular technique to scrutinize the elemental composition and chemical states,^[77] offering the valuable insights into the film's stability and electronic properties. Understanding the optical properties of perovskite thin films is essential for improving their performance in diverse applications, especially in photovoltaics. The UV-Visible (UV-Vis) spectroscopy plays a pivotal role in exploring the optical properties of the perovskite films, providing the valuable information regarding their absorption and transmission characteristics over a wide spectrum range. By analyzing the absorption spectrum in the UV-Visible region, the researchers can identify the onset of absorption, corresponding to the energy required for electronic transitions within the material. In addition, it is useful to determine the band gap of the perovskite materials, a critical parameter to influence the optoelectronic performance of the device. The electronic properties of perovskite films are probed by utilizing the techniques such as photoluminescence spectroscopy (PL) and conductivity measurements. Significantly, the PL also offers a glimpse of the material's optical properties, including band gap and radiative recombination, whereas conductivity measurements provide information about charge carrier mobility and transport behavior. Moreover, time-resolved techniques such as PL decay measurements help to understand the charge carriers' dynamics and the possible degradation pathways. In the pursuit of improving the stability of perovskite thin films, particularly when confronted with environmental challenges, characterization methodologies often include studies on the impact of moisture, light exposure, and temperature fluctuations. In the nutshell, the methodology for characterizing perovskite thin films is a multidimensional approach that includes XRD, SEM, AFM, XPS, UV-Vis spectroscopy, PL, conductivity measurements, and so on. This intricate combination of techniques yields a comprehensive understanding of the structural, compositional, and morphological aspects, ultimately leading to the optimization of perovskite thin films for diverse optoelectronic applications.

3.2. PSCs

Hybrid halide PSCs have progressed at a breakneck pace, allowing them to compete in PCE with single-crystal Si solar cells in just a few years. The high PCE (up to 26.1%)^[16] along with the low-cost processes for the fabrication of PSCs have attracted the attention of many scientists worldwide. The basic working principle for the PSCs involves the charge carrier generation, separation, and transportation toward the respective electrode. The light first falls on the perovskite blend that is sandwiched between the two functional layers (ETL/HTL), resulting in the formation of charge carriers (electron/hole). The total PCE of solar cells, which is defined as the percentage of incoming solar energy that is transformed into electrical power, is often regarded as the most important performance metric for PV systems. The current–voltage (I – V) characteristic is a typical approach to assess solar cell performance. Outdoor testing in natural environments replicates reality and is, in that sense, an ideal circumstance. However, the intensity of incident solar radiation, angle of incidence, albedo, spectral distribution, temperature, and wind speed and direction vary so widely and so quickly that the scientific requirement of repeatability is rarely met. As a result, conducting outdoor tests to satisfy precisely defined test circumstances is impossible. In this regard, for the characterization of PV devices, simulated light is usually taken into account. A solar simulator could be useful for testing small prototyping devices made in research laboratories, especially if it could customize the irradiation at any wavelength interval. A solar simulator referred to the artificial sun, consists primarily of a light source, usually a xenon arc lamp, and a collection of filters designed to ensure that the output light's spectral distribution is as close to the normal AM 1.5G (global) spectrum as possible. Furthermore, to obtain I – V characteristics and external quantum efficiency of solar cell modules, solar simulators are utilized to illuminate the cells while measuring their attributes. **Figure 8**^[78] depicts the comparison of the solar spectrum of AM 1.5G with the spectrum of a xenon lamp solar simulator.

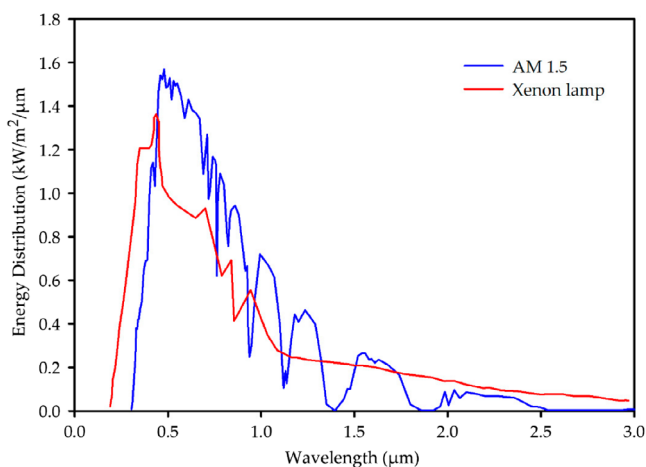


Figure 8. Comparison of AM 1.5G spectrum (blue line) with xenon lamp solar simulator spectrum (Red line).^[78]

4. Chronological Work on Stability of PSCs

Even though most of the leading laboratories have achieved the PCE of lab scale PSCs above 25%, but grave questions are incessantly knocking on the doors of the research laboratories; foremost is, when will these PSCs be utilized for commercial endeavors? Notably, the stability of the solar cell modules is one of the formidable obstacles in the path to commercial success. In this regard, numerous research specialists from all around the world are continuously making significant efforts to improve the stability of PSCs. The perovskite layer is highly sensitive to external environmental conditions such as moisture and oxygen, resulting in the rapid decomposition of PSCs. Furthermore, the stability issue in PSCs also arises from UV and visible radiations but most of these were reported in ambient air condition.^[79–81] Thus, illumination of light significantly triggers the disintegration caused by moisture and provides additional thermal energies and charges.^[82,83] Hence, for PSCs to be stable over time, the need for a superior perovskite layer is imperative and for this, the degradation factor needs to be addressed first. In general, the chemical components, crystal structure, and film quality of perovskites, all these factors affect the stability of the perovskite layer.

Furthermore, based on the change in lattice shape brought on by distortions, perovskites can be classified into three phases, “the cubic phase ($a = b = c$), the tetragonal phase ($a = b \neq c$), and the orthorhombic phase ($a \neq b \neq c$)”. By taking the tolerance factor into account, it is possible to evaluate the structural formability of the 3D ABX₃ type perovskite structures. In addition, the formula for tolerance factor (t) provides the geometric requirement for the formation of an ideal cubic perovskite structure, which is given by the formula

$$t = \frac{R_A + R_X}{\sqrt{2}(R_B + R_X)} \quad (1)$$

in turn, R_A , R_B , and R_X are the radii of A, B cation, and X anion, respectively. However, the ionic radii for some of the ions as illustrated in **Table 1**.^[8] By fully/partially replacing the ions with different sized ions, the t -factor can be changed to produce a cubic crystal structure that is even more stable. For t between 0.8 and 1, ideal cubic structures or perovskite structures with tilted octahedra are preferred. More specifically, if t lies in the range, 0.8–0.9, a distorted perovskite structure forms, whereas for $t = [0.9–1]$, the cubic perovskite structure^[84] dominates. For instance, the most prominent perovskite MAPbI₃ has a tolerance factor of 0.91 and forms the tetragonal structure at room temperature but achieves the ideal cubic structure at elevated temperature (300 K). Furthermore, the stability of PSCs is also determined by another factor known as the octahedra factor, which is specified by the formula

$$\mu = \frac{R_B}{R_X} \quad (2)$$

according to numerous earlier investigations, it is discovered that the value of the t -factor/ μ -factor for 96% halide perovskite lies in the range of 0.813–1.107/0.442–0.895.

Table 1. Ionic radii for some important A, B, and X ions for PSCs.

'A' cation	Radius [pm]	B cations	Radius [pm]	X anions	Radius [pm]
Ammonium [NH ₄] ⁺	146	Pb ²⁺	119	Cl [−]	181
Methylammonium [(CH ₃)NH ₃] ⁺	217	Sn ²⁺	69	Br [−]	196
Azetidinium [(CH ₂) ₃ NH ₂] ⁺	250			I [−]	220
Formamidinium [NH ₂ (CH)NH ₂] ⁺	253				
Dimethylammonium [(CH ₃) ₂ NH ₂] ⁺	272				
Ethylammonium [(C ₂ H ₅)NH ₃] ⁺	274				
Guanidinium [C(NH ₂) ₃] ⁺	278				
Tetramethylammonium [(CH ₃) ₄ N] ⁺	292				
Cs ⁺	167				
Rb ⁺	152				
K ⁺	137				

4.1. MA-Based PSCs

All the extensive research that is currently in perpetuation, in the perovskite PV field, was initiated with the methyl ammonium lead iodide (MAPbI₃). In fact, it is the most researched photoactive material in this field. MAPbI₃ has attracted huge attention from various research groups worldwide due to its exclusive physical and chemical properties. In addition, MAPbI₃ demonstrates an inverted band structure, and the MA⁺ ion contribution to the electronic states is distant from the band edges. To put it another way, empty and occupied states of CB and VB, respectively, are well aligned. MAPbI₃ and similar structures are direct band gap semiconductors exhibiting large optical absorption and luminescence.

The chronological advances in PCE and stability of PSCs with different MA - based perovskite absorber are shown in **Table 2**. As we discussed earlier, Miyasaka and his co-worker for the first time in 2009^[14] investigated HHP CH₃NH₃PbI₃ and CH₃NH₃PbBr₃ as a visible light sensitizer on mesoporous (meso) TiO₂ film and obtained PCE of 3.81% and 3.13%, respectively. However, in the stability test, continuous illumination of light resulted in a photocurrent degradation for an open cell exposed to air. The use of liquid electrolytes as an HTL was the root of device instability. Thus, in 2012, Kim et al.^[23] employed the solid Spiro-OMeTAD as an HTL and fabricated a solid-state mesoscopic heterojunction solar cell. Under illumination with standard AM-1.5G sunlight, they reported a PCE of 9.7%. The device stability was remarkably improved with the use of a solid HTL. They reported, in the long-term stability test in air, that the device was stable for over 500 h at room temperature without encapsulation. Afterward, it grabbed the attention of the scientific community worldwide, and extensive research efforts were started. Further, in the same year, Snaith et al.^[15] achieved a PCE of 10.9% for meso-superstructured solar cell. This

Table 2. Chronological advances in stability and PCE of PSCs with different MA-based perovskite absorber layer.

Perovskite Layer ^{a)}	PCE [%]	Stability	Condition	Year	References
MAPbI ₃	9.7	Stable for 500 h	In air at room temp.; Unencapsulated	2012	[23]
MAPb(I _{1-x} Br _x) ₃	12.3	No loss after 20 days	Under ambient conditions; with RH 35% (55% on the 4th day)	2013	[85]
MAPb(I _{1-x} Br _x) _{3-y} Cl _y	11.1	80% stable for 720 h	N ₂ filled glove box; under dark conditions	2014	[86]
(5-AVA) _x (MA) _{1-x} PbI ₃ ; [5-ammoniumvaleric acid (5-AVA) iodide]*	12.8	Stable for >1000 h	In ambient air under full sunlight; room temp.	2014	[24]
MAPbI _{3-y} Cl _y	15.1	Maintained 95% of initial PCE after 720 h (30 days)	In argon filled glove box; Without encapsulation	2014	[148]
MAPbI _{3-x} (SCN) _x	11.07	92% of initial PCE after 1 h	Upon continuous 1 sunlight illumination	2015	[149]
CH ₃ NH ₃ PbI _{3-x} Cl _x ; [0.5 vol% of EAI] *	10.2	Stable around 80% for over 360 h	Under accelerated heating (65 °C) in a dark condition of Ar environment	2015	[150]
MAPbI ₃ ; [With 4-ABPCI] *	16.7	Stable output over 1 week	Under 10% simulated sun light soaking or 55% humidity in dark	2015	[151]
MAPbI ₃	18.3	More than 90% of initial PCE after 1000 h	Short-circuit condition, under 1 sun illumination	2015	[42]
CH ₃ NH ₃ PbI _{3-x} (SCN) _x	15.1	Retained over 85% of original PCE after 500 h	Without encapsulation; stored in open air; RH ≈70%	2016	[87]
CH ₃ NH ₃ PbI _{3-x} Cl _x ; [PVP/CYTOP]*	12.7	81.2% stable after 820 h	In air; Temp. 22–25 °C; RH ≈24–30%	2016	[152]
MAPbI ₃ ; [PEG]*	≈16.0	Stable for 300 h	High relative humidity 70%, unencapsulated	2016	[153]
MAPbI ₃ ; [3% FEAI]*	18	92% stable for 2880 h (120 days)	In air at room temp.; unencapsulated	2016	[109]
MAPbI ₃ [HCl]*	17.9	16.9% PCE after 30 days	In air at room temp.	2016	[110]
MAPbI ₃	20.3	No loss after 120 h	Air condition, RH ≈40%	2016	[154]
MAPbI ₃ [With ionic Liquid MAAc + TSC]*	19.19	90% of initial PCE after 1000 h 80% of initial PCE after 500 h	With continuous light soaking under simulated AM 1.5 irradiance Thermal test (constant temperature of 85 °C)	2017	[155]
MAPbI ₃	21.2	93.3% after 1000 h of full sun illumination	Under 1.5G Illumination with metal halide lamp including UV radiation, with encapsulation	2017	[96]
MAPbI ₃	19.6	90% of initial PCE after 720 h (1 month)	Ambient conditions (RH 50–60 °C), without encapsulation	2018	[156]
MAPbI ₃	20.1	80% of initial PCE after 760 h	Ambient air, under harsh heat conditions of 85 °C, without encapsulation	2018	[157]
MAPbI ₃	19.56	More than 96% of initial PCE after 100h	Under an elevated temperature of 95 °C, without encapsulation, N ₂ environment	2018	[158]
MAPbI ₃	20.13	More than 70% of initial PCE after 500 h	Ambient condition, 1 sun continuous illumination; without encapsulation	2018	[159]
MAPbI ₃	12.5	No loss over 4000 h	Under continuous 1 sun illumination from xenon lamp-based solar simulator (no UV filtering)	2019	[160]
MAPbI ₃	19.41	80% of initial PCE after 720 h	Ambient air, RH ≈ 45% under dark; without encapsulation	2019	[161]
MAPbI ₃	20.25	86% of initial PCE after 1300 h	At 85 °C under dark; with encapsulation	2019	[162]
MAPbI ₃	20.1	90% of initial PCE after 1000 h	With RH 45% at 85 °C, with encapsulation	2019	[163]
MAPbI ₃	10.01	90% of initial PCE after 1 month	Ambient air (Temp: 25 °C, RH:20–40%), without encapsulation	2020	[164]
MAPbI ₃	16.77	85% of initial PCE after 1000 h	Without encapsulation; at 25 °C, RH ≈ 50%	2020	[165]
MAPbI ₃	17.17	96% of initial PCE after 2000 h	With encapsulation; Ambient condition; 80% RH, 30 °C	2020	[166]
MAPbI ₃ [BZACl]*	19.8	90% of initial PCE after 30 days	Ambient air, RH ≈ 45%; Without encapsulation	2021	[167]
MAPbI ₃ [MAOCN]*	21.28	Retained 95% of initial PCE after 30 days	Ambient air, RT, RH ≈ 10%; without encapsulation	2021	[168]
MAPbI ₃ ; [4TA]*	20.24	Maintained 93% of initial PCE over 30 days	Without encapsulation ; in air; humidity ≈ 55%	2022	[169]
MAPbI ₃ [PEABr]*	19.24	83% of initial PCE after 30 days	In N ₂ filled glove-box; without encapsulation	2022	[170]
MAPbI ₃	18.82	95.7% of initial PCE after 1000 h 92.4% of initial PCE after 1340 h	Under continuous illumination at maximum power point condition at temp. 55 ± 5 °C. Ambient atmosphere, temp. 85 °C, RH ≈ 85%	2022	[171]
MAPbI ₃ [DMDCS]*	20.69	More than 80% of initial PCE after 1000 h	In ambient air; RH ≈ 40%, without encapsulation	2023	[172]

^{a)}* = Additive, RH = Relative Humidity.

efficiency enhancement was accomplished by the use of a wide band gap (7–9 eV) insulator Al_2O_3 that acts as a scaffold. It has also been shown that it is feasible to augment the intrinsic stability of halide perovskite by changing the stoichiometry to halide anions. Therefore, Noh et al.^[85] tuned the chemical composition of halide anion of $\text{MAPb}(\text{I}_{1-x}\text{Br}_x)_3$ perovskites by replacing I^- with Br^- . As iodide contained metal halide was more vulnerable to humidity, they examined the $\text{MAPb}(\text{I}_{1-x}\text{Br}_x)_3$ ($x = 0, 0.06, 0.20, \text{ and } 0.29$) without any encapsulation under ambient conditions while maintaining the 35% humidity for 20 days but a high relative 55% humidity on 4th day as shown in **Figure 9b**. Whereas, as illustrated in **Figure 9a**, higher iodide concentration with respect to bromine has larger absorbance. Interestingly, the $\text{MAPb}(\text{I}_{1-x}\text{Br}_x)_3$ ($x = 0, 0.06$) with less Br concentration based hybrid solar cells experienced serious degradation of PCE after exposure to 55% humidity, whereas their PCE showed great stability for higher Br concentration ($x \geq 0.2$) under inspection for 20 days. The less sensitivity to humidity may be linked with the transformation from the tetragonal phase of MAPbI_3 to a compact and stable cubic phase due to the replacement of larger I atoms with smaller Br atoms. Further in 2014, Suarez et al.^[86] studied the performance of MAPbX_3 derivatives by insertion of Br and Cl and partially replacing the iodide. They prepared the devices of $\text{MAPb}(\text{I}_{1-x}\text{Br}_x)_{3-y}\text{Cl}_y$ on different mesoporous scaffold TiO_2 and Al_2O_3 thin films. They observed the low charge recombination rate for the Al_2O_3 electrode in comparison with the sample prepared on mesoporous TiO_2 . Additionally, they examined the tuning of the bandgap of MAPbX_3 from 1.57 to 2.229 eV by altering the Br concentration ($X = \text{Br}_y\text{I}_{1-y}$, y ranges from 0 to 1) and improved lifetime of devices. Whereas, the device without Br demonstrated an efficiency drop of around 20% of the initial PCE (11.1%) examined inside the glovebox under an N_2 environment and dark conditions. Poor stability due to moisture hindered the success of PSCs in industrial applications since a controlled environment is needed for device operation and fabrication. Thus, in 2016, Yan and co-workers^[87] employed the $(\text{PbSCN})_2$ (lead (II) thiocyanate) in the fabrication of PSCs in ambient air. In comparison with MAPbI_3 , high-quality $\text{CH}_3\text{NH}_3\text{PbI}_{3-x}(\text{SCN})_x$ film was prepared in relative humidity over 70% on meso- TiO_2 by a two-step sequential

deposition method. This unencapsulated device showed much more stability than the PbI_2 precursor-based device. The average PCE obtained was over 13%, with a maximum value exceeding 15% and the device retained 85% of PCE for more than 500 h in ambient air.

It was also adequately reported that the HTL was also a critical part of stable and highly efficient PSCs. In a broad sense, HTL can be classified into four types: small molecules, organic, inorganic, and polymeric.^[88] Small molecules HTL often exhibit the merits of a highly pure film with reproducibility. The most often employed small molecule HTL among them is Spiro-OMeTAD. However, it has low conductivity and poor hole mobility. Thus, to improve the conductivity, the doping of different additives, e.g., lithium bis(trifluoromethanesulfonyl)imide salt (Li-TFSI) and 4-tert-butyl pyridine (t-BP) were carried out for maximizing the hole mobility along with suppression of charge recombination.^[89] However, the hygroscopic nature of Li-TFSI has exacerbated the degradation of PSCs. A novel structural design HTL, Trux-OMeTAD, was presented by Huang et al.^[90] which had immense hole mobility, proper surface energy, and aligned boundary energy level with the perovskite absorbing layer. They fabricated a p-i-n architecture PSC device using Trux-OMeTAD as a p-layer, which demonstrated an enhanced PCE of 18.6% with good stability. In addition, polytriarylamine (PTTA) and poly(3-hxylthiophene-2,5-diyl) (P3HT) were tested to substantially improve the device stability.^[91] Zhao et al.^[92] noted that the dopants were vulnerable to the lifetime of the device and also able to enhance the cost. They fabricated an inverted planer PSC by using a non-doped PTTA which exhibited an excellent PCE of 18.11% together with better stability. In 2016, Yang and coworkers^[93] employed a p-type $\text{NiO}(x)$ as an HTL along with ZnO nanoparticles as ETL, on solution-processed lead halide PSCs. The p-i-n device structure and energy band alignment are depicted in **Figure 10a** which showed an uncertified maximum PCE of 16.1%, with an average of 14.6%. They reported that the device retained about 90% of the initial efficiency after 60 days in the air at room temperature as shown in **Figure 10b** whereas PCE of the device with PEDOT:PSS as HTL degraded abruptly. Ultimately, HTL is significantly vital

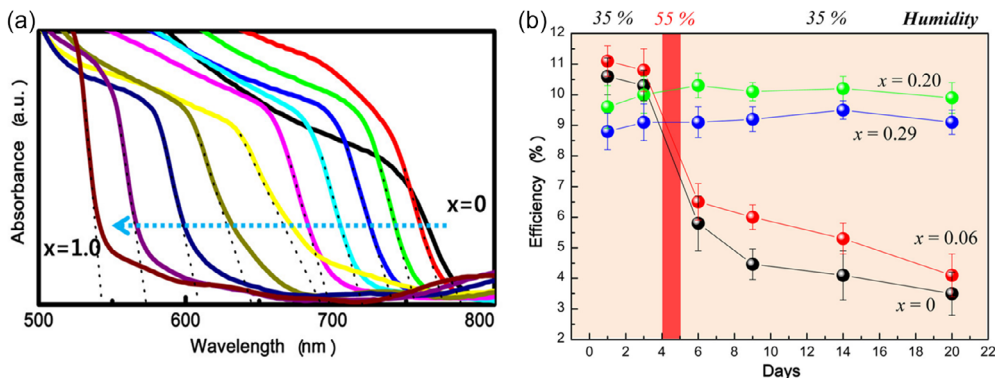


Figure 9. a) UV-Vis absorption spectra of $\text{MAPb}(\text{I}_{1-x}\text{Br}_x)_3$ ($x = 0, 0.06, 0.13, 0.20, 0.29, 0.38, 0.47, 0.58, 0.71, 0.84, 1.0$). b) PCE variation of $\text{MAPb}(\text{I}_{1-x}\text{Br}_x)_3$ ($x = 0, 0.06, 0.20, 0.29$) with number of days. The samples were stored in air without encapsulation at room temperature but with controlled humidity of 35% for 20 days, but 55% on the 4th day.^[85]

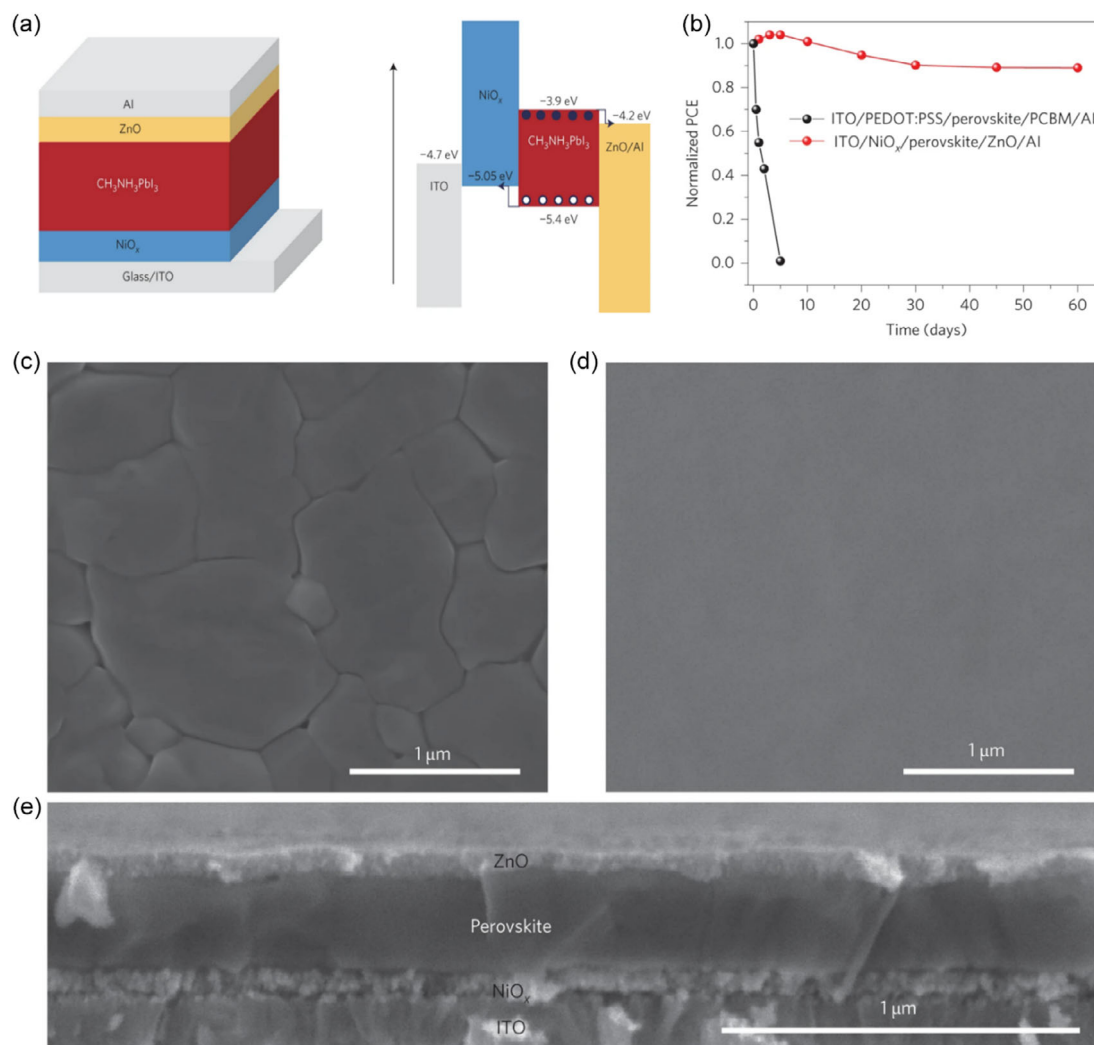


Figure 10. a) Device architecture and energy band alignment of PSC, b) normalized PCE comparison of ITO/PEDOT:PSS/perovskite/PCBM/Al (black) and ITO/NiO_x/perovskite/ZnO/Al (red) structures as a function of storage time in an ambient environment (30–50% humidity, $T = 25\text{ }^{\circ}\text{C}$), c) perovskite layers SEM image grown on a NiO_x surface, d) perovskite coated with ZnO films, e) cross-sectional image of a device (without Al electrode contact).^[93]

to the construction of devices since it directly influences their performance and stability.

A lot of work has also been done on the ETL for advancement in stability of PSCs. The prevalent TiO₂ layer requires a high temperature above 400 °C for deposition.^[94] Therefore, Dong et al.^[95] in 2014 deposited a ZnO film by atomic layer deposition method at 70 °C and achieved a PCE of over 13%. In addition, in 2017, Seok and his group member^[96] investigated the completely novel ETL, lanthanum (La)-doped BaSnO₃ (LBSO), and achieved an outstanding PCE of 21.2% with MAPbI₃ as an absorbing layer. It was reported that LBSO-based PSC was highly stable and maintained over 93% of the original PCE after full sun illumination for 1000 h. Apart from these, SnO₂,^[97–99] Zn₂SnO₄,^[100] CdSe,^[101] MoS₂,^[102] WO₃,^[103] and ZrO₂^[104] were also used as ETL to fabricate PSC devices. Further, some more techniques were also been investigated to improve the lifetime of the devices. Amongst all, solvent engineering,^[105–107] additive engineering,^[108–110] and interface engineering^[111,112] are the most useful approaches.

4.2. FA-Based PSCs

An absorber layer is the heart of the solar cell that can determine perovskite structure and its stability. Although, MAPbI₃ performed quite well as an absorber layer and offered an outstanding efficiency, but there were several issues with it in the context of stability. MAPbI₃ is highly hygroscopic as it decomposed into MAI salt and PbI₂ phase.^[113] The removal of metal halide further accelerated the device deterioration. In place of MA⁺, when a bigger formamidinium ion (HC(NH₂)₂⁺) was substituted, the tolerance factor got increased to 0.99. The FA ion inclusion slightly decreased the band gap to 1.49 eV, from 1.59 eV for MAPbI₃, as its larger size expanded the lattice and slanted the lead iodide octahedra.^[6,114,115] It was observed that FA cations' interactions with PbI₆ octahedra were stronger than those of MA cations because FA was more likely to form hydrogen bonds.^[116] The formation of hydroiodic acid (HI) was also reported when MAPbI₃ was exposed to light by releasing proton from MA cation

with Γ^- . Whereas, due to the resonance property of FA^+ through N–C bonds, FA cation released less proton.^[117] Therefore, FAPbI_3 was considered to have more photostability than MAPbI_3 .

Beginning with the original FAPbI_3 perovskite in 2014, and advancing to different A-site cationic mixtures and various mixed halide analogs, the stability of the HHPs solar cells was improved consistently and ultimately reached up to 4000 h. Several milestones are noteworthy in the stability roadmap of FA-based HHP solar cells: In 2015, Leyden et al.^[118] fabricated the FAPbI_3 -based PSCs using the chemical vapor deposition technique and investigated the effect of perovskite film's chlorine content on the stability of PSCs. Also, perovskite with FAI was found to be more thermally stable than MAI containing perovskite as shown in **Figure 11a**. The resulting device achieved an overall efficiency of 14.2% and retained a PCE of 11.8% after being kept in nitrogen filled glove box for 155 days without encapsulation. Thereafter, in 2016, Zhao and co-workers reported PSCs with an incredible advancement in efficiency and stability by introducing benzylamine in the perovskite film as a surface passivating molecule.^[119] Impressively, the addition of benzylamine considerably improved the resulting device's moisture resistance and enhanced its electronic properties as shown in **Figure 11**. As a matter of fact, PSCs based on benzylamine-modified perovskite film revealed a PCE of 19.2% and sustained no degradation even after 2800 h (4 months) of air exposure. Further, in 2017, a 19.9% overall PCE was reported for $(\text{FAPbI}_3)_{0.97}(\text{MAPbBr}_3)_{0.03}$ based perovskite device with an efficient solution-processed SnO_2 ETL. Under dry air conditions, these cells displayed stability for 40 days.^[99] As listed in **Table 3**, inorganic cesium (Cs) cation

was partially substituted in the FA site of $\text{FAPb}(\text{I}_{1-x}\text{Br}_x)_3$ perovskite by McGehee and his group in the same year,^[120] thus, resulting in better thermal stability. The properly encapsulated device maintained over 90% of its initial PCE ($\approx 14\%$) after passing through 200 temperature cycles between -40 and 85°C .

Undoubtedly, major efforts have been made by material scientists worldwide in subsequent years to develop highly efficient and more stable perovskite-based PV devices. Significantly, Liu et al.^[121] notified Cs/FA mixtures in perovskite films in 2018, demonstrating the better ambient stability of PSCs based on the silica encapsulation approach. Consequently, the resulting PSC with a generic form $\text{FA}_{0.85}\text{MA}_{0.15}\text{PbI}_3$ of perovskite material exhibits a PCE of 18.8% and impressive stability with 97% retention even after 1000 h storage in an ambient environment (25°C ; 10% relative humidity). Furthermore, a highly effective and more thermally stable PSC was fabricated by Jeon et al.^[122] by taking into account the fluorene-terminated HTL. Additionally, they incorporated MAPbBr_3 into FAPbI_3 perovskite, which produced a certified PCE of 23.2% and improved thermal stability compared to the device using Spiro-OMeTAD as the HTL, retaining nearly 95% of its initial PCE for more than 500 h following thermal annealing at 60°C . Also, under continuous illumination, this encapsulated device maintained 92.6% of initial PCE after 310 h. Further, Lin et al.^[123] observed that the efficiency of p-i-n structured PSCs, with organic ETL and HTL, was improved by an ionic solid, a piperidinium salt. Further, during aggressive aging, the supplement inhibited compositional separation into impurity phases and pinhole production in the perovskite active material. By incorporating the additive $[\text{BMP}]^+[\text{BF}_4]^-$, the final device, with and without encapsulation, was able to successfully maintain 95% and 80% of its original PCE under full light

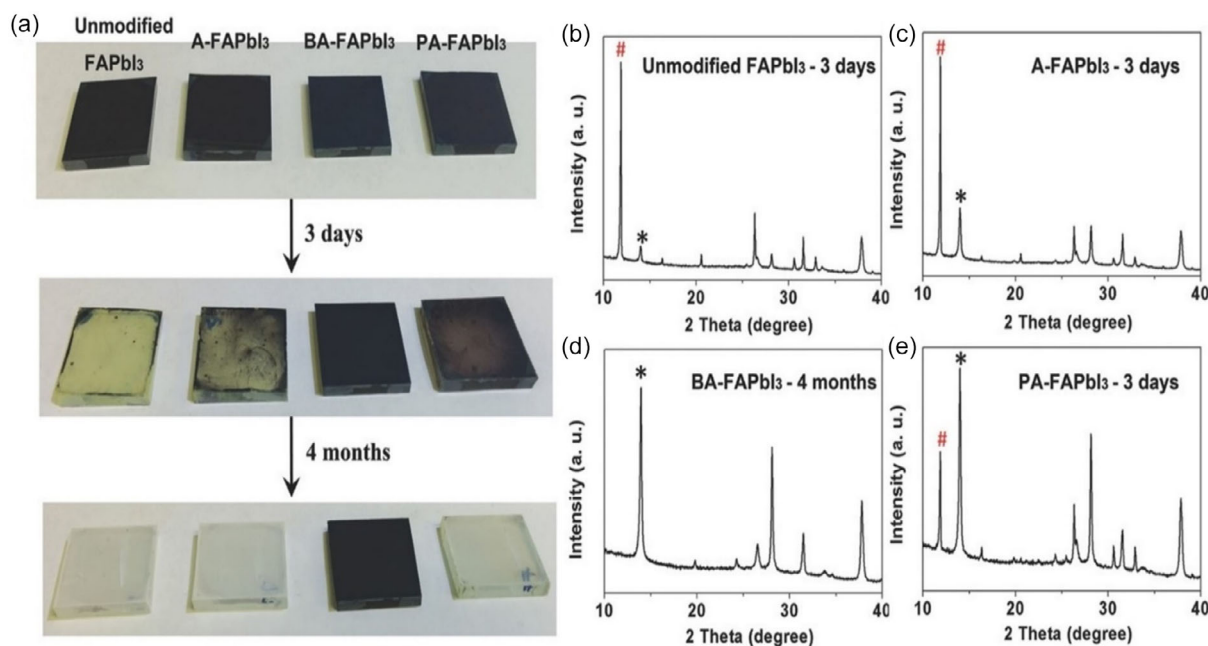


Figure 11. a) Images of unmodified FAPbI_3 , A- FAPbI_3 , BA- FAPbI_3 , and PA- FAPbI_3 films for different durations of exposure (fresh, 3 days, 4 months) under 50 ± 5 RH% air. b–e) XRD patterns of unmodified FAPbI_3 , A- FAPbI_3 , BA- FAPbI_3 , and PA- FAPbI_3 films after same exposure in moisture air. Except for the BA- FAPbI_3 film, which was exposed for 4 months, all other films were exposed for 3 days. * and # highlight the XRD peaks corresponding to the (110) plane of α - FAPbI_3 and δ - FAPbI_3 , respectively.^[119]

Table 3. Chronological advances in stability and PCE of PSCs with different FA-based perovskite absorber layer.

Perovskite Layer ^{a)}	PCE (%)	Stability	Condition	Year	References
FAPbI ₃	14.2	PCE 11.8% after 155 days	Nitrogen-filled glove box; unencapsulated	2015	[118]
FA _{0.9} CS _{0.1} PbI ₃	16.5	67% degradation after 30 min	N ₂ filled glove box; with illumination; Encapsulated	2015	[117]
MA _x FA _{1-x} PbI ₃	≈13.6	Stable for 30 days	Inert atmosphere in the glove box and under illumination	2015	[173]
FAPbI ₃	11.44	Maintained 87% of initial PCE after 1 h	Under continuous light illumination (AM1.5 global solar light at 100 mW cm ⁻²); without encapsulation; RH ≈ 30–40%	2016	[174]
FAPbI ₃	19.2	No loss after >2800 h	Ambient air with RH ≈ 50 ± 5%	2016	[119]
(FAPbI ₃) _{0.97} (MAPbBr ₃) _{0.03}	19.9	Stable for 40 days	Dry air condition	2017	[99]
CS _{0.17} FA _{0.83} Pb(I _{0.83} Br _{0.17}) ₃	≈14	Maintained 90% of initial PCE after 200 temperature cycle	Temperature cycle between -40 and 85 °C; with encapsulation	2017	[120]
FA _x MA _y CS _{1-x-y} Pb(I _{1-z} Br _z) ₃	12.2	Maintained approximately 88% of avg. initial PCE after 1000 h	Ambient air; continuous operation with no ultraviolet filtering	2018	[125]
CS _{0.05} FA _{0.81} MA _{0.14} PbBr _{0.45} I _{2.55}	19.89	>80% after 700 h	Ambient air	2018	[175]
FA _{0.85} CS _{0.15} PbI ₃	18.8	97% retention after 1000 h	25 °C; 10% RH	2018	[121]
CS _{0.17} FA _{0.87} Pb(I _{0.83} Br _{0.17}) ₃	16.43	No loss after 14 h	Ambient condition; continuous 1 sun illumination; RH ≈ 50%	2018	[176]
CS _{0.17} FA _{0.83} Pb(I _{0.83} Br _{0.17}) ₃	>14	Maintained 99% of initial PCE after 1000 h	Damp-heat test(Temp. 85 °C, RH ≈ 85%); with encapsulation	2018	[177]
(FAPbI ₃) _{0.95} (MAPbBr ₃) _{0.05}	23.2	Maintained 95% of initial PCE for more than 500 h Maintained 92.6% of initial PCE after 310 h	Thermal stress at 60 °C temp. Encapsulated; under continuous illumination	2018	[122]
(FAPbI ₃) _{0.95} (MAPbBr ₃) _{0.05}	22.7	Maintained 80% of initial PCE after 1008 h 95% retained after 1370 h	85% RH; room temp.; unencapsulated 1 sun illumination; encapsulated	2019	[128]
CS _{0.05} (FA _{0.85} MA _{0.15}) _{0.95} Pb(I _{0.85} Br _{0.15}) ₃	20.9	Maintained 90% of initial PCE after 700 h	Encapsulated; temp. 85 °C; RH≈85%	2019	[178]
CS _{0.05} (FA _{0.92} MA _{0.08}) _{0.95} Pb(I _{0.92} Br _{0.08}) ₃	21.2	No loss after 1000 h	Encapsulated; under AM 1.5G illumination	2020	[179]
CS _{0.17} FA _{0.83} Pb(I _{0.77} Br _{0.23}) ₃	17.3	Maintained 80% of initial PCE after 1010 h Maintained 95% of initial PCE after 1200 h	Ambient air; temp. 60 °C; RH ≈ 50%; full spectrum sunlight; without encapsulation Ambient air; temp. 85 °C; full spectrum sunlight; with encapsulation	2020	[123]
FAPbI ₃	24.82	87% efficient after 500 h	RH ≈ 50%; without encapsulation, ambient air	2020	[180]
CS _{0.05} (FA _{0.85} MA _{0.15}) _{0.95} Pb(I _{0.85} Br _{0.15}) ₃	22.02	Maintained 90% of initial PCE after 1100 h Maintained 92% of initial PCE after 1000 h	Ambient condition; RH ≈ 75% 1 sun illumination; Temp. 85 °C; N ₂ filled glove box; with encapsulation	2020	[181]
CS _{0.05} FA _{0.8} MA _{0.15} Pb(I _{0.85} Br _{0.15}) ₃	19	No loss after 1800 h No loss after 75 cycles	Damp heat test(-40 to 85 °C) Humidity freeze testing (RH≈85%)	2020	[182]
CS _{0.1} FA _{0.9} PbI ₃	12.3	Maintained 90% of initial PCE for over 800 h	Under continuous light illumination; Dry N ₂ filled glove box	2020	[183]
FA _{1-x} MA _x PbI ₃	18.8	Maintained 90% of initial PCE after 1 month (720 h)	Under 1 sun illumination; Dry N ₂ environment; Temp. 25 °C	2020	[184]
CS _{0.05} MA _{0.14} FA _{0.81} PbI _{2.55} Br _{0.45}	19.6	Showed 89% of initial PCE after 1000 h	Without encapsulation; ambient air; 25 °C Temp.; RH ≈ 25%	2020	[185]
(FAPbI ₃) _x (MAPbBr ₃) _{1-x}	23.0	Maintained more than 85% of initial PCE after 2000 h	Ambient condition; continuous light illumination	2021	[124]
CS _{0.05} (FA _{0.85} MA _{0.15}) _{0.95} Pb(I _{0.85} Br _{0.15}) ₃	21.4	Retained 80% after 4000 h	N ₂ atmosphere; continuous 1 sun illumination	2021	[126]

Table 3. Continued.

Perovskite Layer ^{a)}	PCE (%)	Stability	Condition	Year	References
Cs _{0.15} FA _{0.85} Pb(I _{0.95} Br _{0.05}) ₃	22.3	Maintained 97.5% of initial PCE after 1000 h	Continuous 1 sun illumination with maximum power point tracking at 45 °C; without encapsulation	2022	[186]
Cs _x FA _{1-x} PbX ₃	24.1	Maintained 80% of initial PCE after 1000 h 80%/78% of initial PCE after 500 h	Under continuous light illumination in N ₂ environment; without encapsulation Thermal treatment at 70 °C/85 °C	2022	[187]
FAPbI ₃	23.94	95% of initial PCE after 100 days 90% of initial PCE after 1050 h	Ambient air with RH ≈ 20–30% in dark, without encapsulation Under constant 1 sun illumination in N ₂ environment at room temperature	2022	[188]
FA _{0.85} MA _{0.15} PbI ₃	24.29	91% of initial PCE after 1440 h 83% of initial PCE after 500 h	Ambient air; without encapsulation Under N ₂ atmosphere at 85 °C; without encapsulation	2022	[189]
FA _{0.15} MA _{0.85} PbI ₃	22.54	92% of initial PCE after 400 h	Without encapsulation; ambient conditions; 25 °C Temp.; RH ≈ 10–20%	2023	[190]
Cs _x FA _{1-x} PbX ₃	23.6	Maintained 95% of initial PCE after 2200 h 92% of initial PCE after 250 h	After illumination in MPP conditions at room temperature; with encapsulation Under MPP tracking at 85 °C under atmospheric conditions	2023	[191]
FA _{0.9} Cs _{0.1} PbI ₃	24.64	89% of initial PCE after 500 h 93% of initial PCE after 500 h 95% of initial PCE after 1500 h	Continuous 1 sun illumination under atmospheric conditions; with encapsulation Thermal treatment at 85 °C in N ₂ environment; without encapsulation Without encapsulation; ambient air; 25 °C Temp.; RH ≈ 25%	2023	[192]

^{a)}RH – Relative humidity, MPP – Maximum power point.

illumination after 1200 and 1010 h of operation at 85 and 60 °C, respectively. It is important to note that organic A-site cations are crucial for structural stability. It impacts the structure indirectly due to their distant electronic levels from the band edge. Therefore, Xue et al.^[124] showed that the extended electronic state, induced by π -conjugation, which altered the perovskite frontier orbital. The resulting device exhibited a PCE of 23% and was able to maintain 85% of the initial PCE after 2000 h of continuous light illumination. Also, Luthar and his colleagues^[125] tested the large composition engineering simultaneously for A-site cation and halide anion. They fabricated a FA_xMA_yCs_{1-x-y}Pb(I_{1-z}Br_z)₃ structure-based PSC and reported improved phase stability compared to FA or CsPbI₃. The best-unencapsulated device, among all the tested devices, retained 94% of original PCE (12.2%) after continuous operation in ambient air even without any UV light filtration. In addition, the PSCs have limited interface stability and life span due to the low formation energies of the absorber layer, which result in low toughness and soft materials. Thus, to increase the mechanical reliability, Dai et al.^[126] used an iodine-terminated self-assembled monolayer that resulted in a 50% enhancement

of interface adhesion toughness between perovskite film and ETL. They optimized the mixed composition perovskite Cs_{0.05}(FA_{0.85}MA_{0.15})_{0.95}Pb(I_{0.85}Br_{0.15})₃ which was 21.4% efficient initially and retained 80% of the original PCE after 4000 h operation in N₂ environment under continuous light exposure. Furthermore, interfacial defects between the charge transporting layer and perovskite light absorbing layer are also responsible for the efficiency and stability declination of PSC devices. These defects impede charge extraction and transportation which significantly decrease the device performance. Therefore, to minimize these interfacial defects, efforts were made globally in various adequate ways, particularly by surface passivation.^[127–129] Recently, Min et al.^[130] passivated the perovskite layer through the formation of an atomically coherent interlayer by linking the Cl-bonded SnO₂ with a Cl-doped perovskite precursor. The interlayers substantially lowered the interfacial defects and enhanced the charge transport property which resulted in the fabrication of a device with a certified PCE of 25.5%. In addition, the device also successfully maintained 90% of the original PCE after 500 h operation under continuous light illumination even without any encapsulation.

4.3. Efficient Large Guanidinium Mixed MA/FA PSCs

Although, a PSC demonstrates an unprecedented rapid development in PCE, close to the predicted theoretical limit, but their long-term stability is still a major challenge that concealed their outstanding efficiency. As we discussed earlier, various efforts have been made in the direction of stability enhancement. In the continuity of A-site cation compositional engineering, several organic cations are indeed being investigated as the possible contenders. In 2015, Giorgi et al.^[131] first studied the thermal stability of perovskites with large GA cations. They theoretically studied the effect of nearly zero dipole moment GA cation $[(\text{NH}_2)_3\text{C}^+]$ by DFT, to counter the hysteresis problem in current–voltage curves as the lead iodide cavity is appropriately filled with its molecular size. The ionic radii of GA along with other organic cations are listed in Table 1. The corresponding tolerance factor of GAPbI_3 can be calculated by the tolerance formula given in Equation (1), which turned out to be 1.04, hence, it is difficult to form GAPbI_3 in pure form.

In 2016, Yang and co-workers^[132] addressed the passivation effect through the partial addition of GA in MAPbI_3 and achieved a PCE exceeding 17% as shown in Table 4. The incorporation of GA resulted in the reduction of defect activation energy and an increment in carrier lifetime within the device. They compared the performance of GA-based devices with pristine MAPbI_3 stored in the dry oxygen environment for 180 h and observed a rapid decrease in original PCE for pure MA-based device. Whereas, the addition of GA exhibited stability of over 80%. Nazeeruddin and his group, in 2017,^[133] tested the thermal stability of $\text{MA}_{1-x}\text{GA}_x\text{PbI}_3$ ($x = 0, 0.125, 0.15, 0.25$) PSC in an argon atmosphere and under continuous light illumination at 60 °C. For $x = 0.25$, the PCE of the device was found to be 17.14% and this device exhibited enhanced stability among all considered compositions, with a slight reduction in PCE even after 1000 h as

shown in Figure 12d. Also, with 14% guanidinium content, they measured average 19.21% PCE in the air under 1 sun illumination as depicted in Figure 12c. Further, in the continued search for an optimal GA amount, Gao et al.^[134] achieved a champion efficiency of 20.38% with a GA fraction of 5.26% in MAPbI_3 . After storage for 900 h at a temperature 20 °C with a relative humidity of 15%, the unencapsulated device retained 90% of its initial PCE in air. Owing to the incorporation of large size GA cation expands the lattice and elongates the Pb–I bond. Consequently, the band gap widening from 1.49 to 1.53 eV was observed. Alloyed A-site cations play a significant role in defining the band gap, crystal structure, and phase stability along with ion migration.

In 2022, Li with his group^[135] studied the activation energy for iodide ion migration with different fractions of GA^+ substitution. They doped an equal amount of FA^+ along with GA^+ in MAPbI_3 and synthesized a triple cation perovskite ($\text{MA}_{0.8}\text{FA}_{0.1}\text{GA}_{0.1}\text{PbI}_3$). It exhibited 22.17% PCE with excellent operational stability with only 10% degradation in efficiency under continuous light illumination for 1200 h. Furthermore, it demonstrated a PCE of 19.18% with the 14 cm² active area mini solar module.^[135] Defects in the perovskite layer may lead to stability and performance reduction as well as hysteresis phenomenon during I – V measurements. Therefore, a passivation treatment was performed through the inclusion of bulky cations GA^+ and phenylethylammonium (PEA^+) acting as additives in MAPbI_3 thin film.^[136] In comparison to the control film, the triple cations perovskite film may have lower trap densities and improved carrier transport as a result of the internal interactions between mixed bulky cations. Therefore, the mixed-cation-based module demonstrated a remarkable PCE of 20.64%. Interestingly, the device retained 62.7% of its initial performance, in ambient surroundings with 60–80% relative humidity, after 720 h of storage.^[136] GA-doped quadruple cation perovskite was also

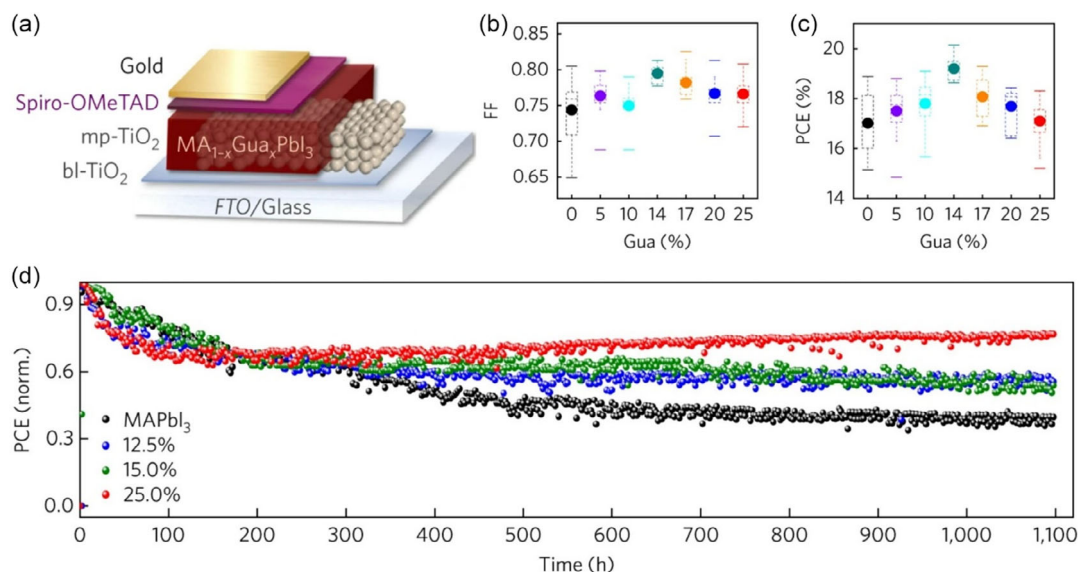


Figure 12. a) Guanidinium (Gua) cation-incorporating PSC device structure, b,c) Fill-factor and PCE vs GA concentration, upper bar, and lower bar represent maximum and minimum value, respectively, and circle shows average PCE value and d) $\text{MA}_{1-x}\text{Gua}_x\text{PbI}_3$ thermal stability test at 60 °C under continuous light illumination.^[133]

studied by Zhang et al.^[137] by tuning the GA concentration in $\text{Cs}_{0.05}(\text{FA}_{0.83}(\text{MA}_{1-x}\text{GA}_x)_{0.17})_{0.95}\text{Pb}(\text{I}_{0.83}\text{Br}_{0.17})_3$ ($x = 0$ to 1) and investigated the corresponding phase, morphology, chemical composition, and stability. A higher fraction of GA induced the 2D phase of FAGAPbI_4 and 1D $\delta\text{-FAPbI}_3$ which had both positive and negative impacts on device performance. The experimental result revealed that $\text{Cs}_{0.05}(\text{FA}_{0.83}(\text{MA}_{1-x}\text{GA}_x)_{0.17})_{0.95}\text{Pb}(\text{I}_{0.83}\text{Br}_{0.17})_3$ ($x = 0.2$) exhibited the champion efficiency of 20.29% with V_{oc} 1.12 V. It had also been observed that the unencapsulated devices at 80 °C and 40% relative humidity, with 0.6 and 0.2 GA content maintained more than 70% and 60% of their original PCE after 1440 h, respectively. Besides, the improved stability was associated with the better passivation effect of 1D/2D phases (Table 4).

4.4. Stability Problems and Its Solution Strategies

Despite the remarkable advancements made in PSCs so far, the main question is still knocking at the door of perovskite research laboratories, how long it will take for the commercialization of the PSCs? The PSCs have emerged as potential contenders for next generation PV technologies owing to their outstanding PCE^[16] and cost-effective fabrication processes.^[8] However, the commercial viability of these PSCs is hindered by inherent

stability challenges. More significantly, preserving the stability of PSCs is more vital for commercialization than increasing PCE close to Shockley–Queisser (SQ) limit at present. Over time, scientists have meticulously investigated the instability issues in these solar cells, seeking to unravel the factors responsible for instability and the effective solution strategies for it.^[138–141] One of the predominant stability concerns revolves around the moisture sensitivity of perovskite materials,^[138] which can lead to degradation over time. To address this, the researchers are actively exploring encapsulation techniques such as the use of advanced moisture-resistant barrier films and hydrophobic coatings to shield the perovskite layer from moisture ingress, ensuring sustained stability in varying environmental conditions.^[141,142] Another critical stability issue is the thermal sensitivity of perovskite materials, making them prone to degradation and performance loss with temperature fluctuations.^[139] The solution strategies include the development of stable perovskite formulations that exhibit reduced sensitivity to temperature changes. Additionally, the integration of thermally robust charge transport materials is being investigated to enhance the overall thermal stability of PSCs.^[143] Furthermore, the vulnerability of PSCs to UV light poses yet another stability issue. Prolonged exposure to UV radiation can cause degradation, lowering the device's efficiency over time.^[139] In this regard, the researchers are investigating the incorporation of UV-stabilizing additives

Table 4. Chronological advances in stability and PCE of PSCs with different GA-based perovskite absorber layer.

Perovskite layer ^{a)}	PCE [%]	Stability	Cond.	Year	References
$\text{GA}_{0.15}\text{MA}_{0.85}\text{PbI}_3$	17.1	80% of initial PCE after 7.5 days (180 h)	Dry oxygen environment	2016	[132]
$\text{GA}_{0.14}\text{MA}_{0.86}\text{PbI}_3$	20.15	Stable over 1000 h	At 60 °C temp. and under Ar atmosphere	2017	[133]
$\text{FA}_{(1-x-y)}\text{Cs}_x\text{GA}_y\text{PbI}_3$	17.7	60% of initial PCE after 180 min of exposure	85% RH, 1 sun illumination in air	2018	[193]
$\text{MAPbI}_3.10\% \text{GASCN}^*$	16.70	90% of initial PCE after 14 days	Without encapsulation	2019	[194]
$\text{Cs}_{0.05}(\text{FA}_{0.83}(\text{MA}_{1-x}\text{GA}_x)_{0.17})_{0.95}\text{Pb}(\text{I}_{0.83}\text{Br}_{0.17})_3$	20.29	60% of initial PCE after 60 days 90% of initial PCE after light-soaking for 300 min	Exposing to an environment of 25 °C, and 25% humidity Under AM 1.5G illumination in ambient environment.	2019	[137]
$\text{GA}_{0.05}\text{Cs}_{0.15}\text{FA}_{0.8}\text{Pb}(\text{I}_{0.85}\text{Br}_{0.15})_3$	21.3	80% of initial PCE after 8 h	Under 1 Sun-illumination	2019	[195]
$\text{GA}_{0.053}\text{MA}_{0.947}\text{PbI}_3$	20.38	90% of initial PCE after 900 h	At a humidity of 15 ± 5% and a temperature of 20 ± 5 °C in air.	2020	[134]
$\text{Cs}_{0.05}\text{GA}_{0.05}\text{MA}_{0.90}\text{PbI}_3$	21.22	50–55% of initial PCE after 600 h	Without encapsulation	2021	[196]
$\text{MAPbI}_3.\text{GAI}^*$	19.25	84% of initial PCE in more than 24 days	Atmospheric environment (temperature: 25–30 °C, humidity: 30–40% RH); without encapsulation	2021	[197]
$\text{MA}_{0.8}\text{FA}_{0.1}\text{GA}_{0.1}\text{PbI}_3$	22.17	90% of initial PCE after 1200 h	Under continuous light-soaking	2022	[135]
$\text{MAPbI}_3.5 \text{ mg mL}^{-1} \text{ GABF}_4^*$	20.54	86% of initial PCE after 150 h	Exposing to continuous 1 sun AM1.5G illumination of Xe-lamp in N ₂ environment at 25 °C, without encapsulation	2022	[198]
85% of initial PCE after 50 days		Without encapsulation			
$\text{MAPbI}_3.\text{GACl}^*/\text{PEACl}^*$	20.64%	82.4% of initial PCE after 720 h 62.7% of initial PCE after 720 h	N ₂ filled glove box at room temperature In an ambient environment with RH of 60–80% at room temperature	2022	[136]
$\text{MAPbI}_3.10\% \text{ GABr}$	16.70%	Retained >97% of initial PCE after 400 h	Under continuous 1 sun illumination at ambient conditions (RH = 60–65% and 34–36 °C)	2023	[199]

^{a)}*. Additive, RH – Relative Humidity.

and protective coatings. These approaches aim to reduce the impact of UV radiation on perovskite stability, thereby extending the operational lifespan of PSCs. In addition, ion migration within the perovskite layer has also been recognized as a cause of the deterioration of PSCs' stability.^[144] Uncontrolled ion movement can result in performance losses over time. Notably, an effective solution to this issue involves the introduction of additives and compositional engineering to reduce ion migration phenomena within the perovskite layer.

Chemical stability remains a persistent challenge since many perovskite materials have inherent chemical instability, resulting in decomposition.^[145] The researchers are dedicated to the continual optimization of perovskite compositions and the investigation of novel materials with enhanced chemical stability. In contrast, the poor interactions between the different layers of PSC architecture result in device instability. Interestingly, interface engineering can be a more fruitful approach to overcome this problem. Various attempts are made continuously to optimize the interface between the charge transport layer and the perovskite materials in order to improve overall device stability.^[146] All these efforts contribute to the continuous evolution of perovskite technology, bringing it closer to widespread commercialization. In the nutshell, addressing the stability challenges of PSCs is pivotal for unlocking their full potential in practical applications. This comprehensive understanding of stability challenges and the corresponding evolution of effective solutions underscore the ongoing efforts to propel PSCs toward commercial viability and widespread adoption in the renewable energy landscape.

5. Challenges and Future Aspects

The wake of global energy crisis, including those related to supply, price, and pollution associated with traditional sources of energy, the international community has been seriously considering the use and development of renewable energy as an alternative solution. Renewable energy, if developed, has potential to supply required energy for economic development at zero environmental cost. The increasing importance attached to the issue is derived from the fact that sustainable development is almost impossible without the use of sustainable energy sources. For a sustainable and efficient energy landscape, a systematic and diligent exploration of domain of renewable energy is vital. Solar energy is poised to become an indispensable part of sustainable energy, but until all the persistent challenges linked with solar energy are surmounted, the promise of pollution-free energy from the sun will remain distant. To harvest more of this free energy, new efficient materials need to be discovered and studied. Pertaining to this, the combinations of perovskite materials explored above can contribute tremendously to the advancement of solar technology under common atmospheric conditions. Since their inception in 2009, persistent improvements have been made in PSCs but the more recent developments in their composition, interface designing, fabrication, and synthesis techniques have led to attainment of a PCE of 26.1%, which is higher than that of DSSC and CdTe-based solar cells. Despite the notable advancement achieved by these solar cells, it is prudent to

acknowledge that their present performance is still far from reaching the potential that PSCs hold.

The critical and intricately connected triad of stability, efficiency, and large scale production requires heightened attention and concerted efforts to propel further advancements in this field. Achieving stability and high efficiency in PSCs involves complexities in navigating the intricacies at multiple levels. To begin with, getting consistency in material quality and reproduction of the fabrication process can be very challenging when the production of PSC is transitioning from laboratory to industry. The venerability of PSC for degradation leaves them susceptible to efficiency reduction. The long term and permanent solutions for existing issues of stability, that allows commercial viability lie in maneuvering the complex process of interface engineering between different layers, quality enhancement in large scale manufacturing processes, and efficient and scalable encapsulation methods. Besides that, working on the development of stable and effective materials for other dominant layers (HTL, ETL) of PSCs is indispensable for further improvement and realization of high performance in these solar cells. Hence, various combinations of materials are yet to be tested from both theoretical and experimental levels for an optimal combination with enhanced efficiency and increased stability.

The exciting future aspects of PSCs lie in their suitability in integration with other solar cell materials like Si or organic materials in the form of tandem solar cell architecture to attain even higher PCE by exploiting the complementary absorption spectra of different materials and maximizing the energy absorption. Developing novel perovskite formulations will definitely aid in engineering strategies to enhance their stability and sustain high performance under all environmental conditions. Further, a priority should be placed on getting more insight into the understanding and controlling of the charge carrier recombination and transport dynamics within these solar cells, necessitating further research efforts. Their ability to integrate with energy storage devices can also be explored to create self-contained solar powered systems. Their flexibility, lightweightness, and semi-transparent nature can potentially change the construction industry by facilitating their use as building-integrated photovoltaics. The advanced algorithms used in ML hold great promise in optimizing perovskite material design, fabrication processes, and identification of optimal parameters, thus, paving the way for more reliable, efficient, and sustainable energy solutions.

6. Conclusion

In the nutshell, it can be concluded that this review opens a new direction by proposing HHP-based solar cell as an alternative of Si solar cells. Although commercially available Si solar cells have quite high efficiency and stability, yet their manufacturing process is very difficult and highly expensive. In addition, DSSCs are available in the market, but their efficiency is still less than 15%. The PSCs, in contrast, are less costly, lightweight, and flexible. Apart from the inexpensive solution-based fabrication process, these perovskites have a huge defect tolerant capacity, and suppressed carrier recombination. After reviewing the literature, we found that various attempts have been made to increase efficiency and stability. This efficiency has been increased

drastically up to 26.1% in a very short interval of time. The HHP-based PSCs are on the right track to yield the desired PCE with the advancement in material developments. These PSCs can be used in tandem solar cells, thereby increasing the PCE to overcome the SQ efficiency limit. As bandgap of the perovskite can be tuned by simply changing composition and hence such materials have good applications in single junction and tandem solar cells. For example, the bandgap of MAPbI₃ can be tuned between the values 1.6–2.3 eV by simply substituting I with Br. Another example is FAPbI₃ with a bandgap in a range from 1.48 to 2.23 eV. Further, the enhancement in efficiency is possible with interface engineering, compositional, and band engineering of materials used in the PSCs. Therefore, among all the PV technologies of the twenty-first century, the PSCs offer a new spark for the advancement of renewable energy sources in terms of solar cells owing to their unique morphological and optoelectronic properties. Nevertheless, in order to attract a market within the industry like Si PV panels, the PSCs must guarantee to yield stable power for a period of around 25 years in outdoor conditions. Thus, in this review, we have analyzed the progress in the operational stability of PSCs and postulated the possible device degradation mechanism. We hope that this review will provide new insights to young researchers toward the long term environmental stability of PSCs and will extend the promotion of their commercialization.

Acknowledgements

The work is supported by Haryana State Council of Science, Innovation and Technology (HSCSIT), Panchkula vide grant no. HSCST/R&D/2019/1306-07. The authors M.K.K., S.D., and P.K.D. are grateful to M/S/ Ultra International Pvt. Ltd., Ghaziabad, India for providing the lab furniture for Renewable Energy Laboratory at SPS, JNU.

Conflict of Interest

The authors declare no conflict of interest.

Keywords

perovskite solar cells, photovoltaics, power conversion efficiency, solar energy, stabilities

Received: November 23, 2023

Revised: January 16, 2024

Published online:

- [1] G. Rose, *De novis quibusdam fossilibus quae in montibus uraliis inve-niuntur*, Typis A. G. Schdii, Berolini **1839**.
- [2] S. Patwardhan, D. H. Cao, S. Hatch, O. K. Farha, J. T. Hupp, M. G. Kanatzidis, G. C. Schatz, *J. Phys. Chem. Lett.* **2015**, *6*, 251.
- [3] H. L. Wells, *Am. J. Sci.* **1893**, *s3–45*, 121.
- [4] M.-H. Jung, S. H. Rhim, D. Moon, *Sol. Energy Mater. Sol. Cells* **2017**, *172*, 44.
- [5] C. C. Stoumpos, M. G. Kanatzidis, *Adv. Mater.* **2016**, *28*, 5778.
- [6] T. Jesper Jacobsson, J.-P. Correa-Baena, M. Pazoki, M. Saliba, K. Schenk, M. Grätzel, A. Hagfeldt, *Energy Environ. Sci.* **2016**, *9*, 1706.

- [7] S. J. Yoon, K. G. Stamplecoskie, P. V. Kamat, *J. Phys. Chem. Lett.* **2016**, *7*, 1368.
- [8] A. K. Jena, A. Kulkarni, T. Miyasaka, *Chem. Rev.* **2019**, *119*, 3036.
- [9] S. De Wolf, J. Holovsky, S.-J. Moon, P. Löper, B. Niesen, M. Ledinsky, F.-J. Haug, J.-H. Yum, C. Ballif, *J. Phys. Chem. Lett.* **2014**, *5*, 1035.
- [10] S. D. Stranks, G. E. Eperon, G. Grancini, C. Menelaou, M. J. P. Alcocer, T. Leijtens, L. M. Herz, A. Petrozza, H. J. Snaith, *Science* **2013**, *342*, 341.
- [11] D. Shi, V. Adinolfi, R. Comin, M. Yuan, E. Alarousu, A. Buin, Y. Chen, S. Hoogland, A. Rothenberger, K. Katsiev, Y. Losovyj, X. Zhang, P. A. Dowben, O. F. Mohammed, E. H. Sargent, O. M. Bakr, *Science* **2015**, *347*, 519.
- [12] G. Xing, N. Mathews, S. Sun, S. S. Lim, Y. M. Lam, M. Grätzel, S. Mhaisalkar, T. C. Sum, *Science* **2013**, *342*, 344.
- [13] W.-J. Yin, J.-H. Yang, J. Kang, Y. Yan, S.-H. Wei, *J. Mater. Chem. A* **2015**, *3*, 8926.
- [14] A. Kojima, K. Teshima, Y. Shirai, T. Miyasaka, *J. Am. Chem. Soc.* **2009**, *131*, 6050.
- [15] M. M. Lee, J. Teuscher, T. Miyasaka, T. N. Murakami, H. J. Snaith, *Science* **2012**, *338*, 643.
- [16] National Renewable Energy Laboratory(NREL), Best Research-Cell Efficiency Chart, <https://www.nrel.gov/pv/cell-efficiency.html> (accessed: August 2023).
- [17] N. Li, X. Niu, Q. Chen, H. Zhou, *Chem. Soc. Rev.* **2020**, *49*, 8235.
- [18] Y. Jiang, L. Qiu, E. J. Juarez-Perez, L. K. Ono, Z. Hu, Z. Liu, Z. Wu, L. Meng, Q. Wang, Y. Qi, *Nat. Energy* **2019**, *4*, 585.
- [19] A. Uddin, M. Upama, H. Yi, L. Duan, *Coatings* **2019**, *9*, 65.
- [20] K. Sharma, V. Sharma, S. S. Sharma, *Nanoscale Res. Lett.* **2018**, *13*, 1.
- [21] C. S. Ponseca, T. J. Savenije, M. Abdellah, K. Zheng, A. Yartsev, T. Pascher, T. Harlang, P. Chabera, T. Pullerits, A. Stepanov, J.-P. Wolf, V. Sundström, *J. Am. Chem. Soc.* **2014**, *136*, 5189.
- [22] B. Chen, N. Ren, Y. Li, L. Yan, S. Mazumdar, Y. Zhao, X. Zhang, *Adv. Energy Mater.* **2022**, *12*, 2003628.
- [23] H.-S. Kim, C.-R. Lee, J.-H. Im, K.-B. Lee, T. Moehl, A. Marchioro, S.-J. Moon, R. Humphry-Baker, J.-H. Yum, J. E. Moser, M. Grätzel, N.-G. Park, *Sci. Rep.* **2012**, *2*, 591.
- [24] A. Mei, X. Li, L. Liu, Z. Ku, T. Liu, Y. Rong, M. Xu, M. Hu, J. Chen, Y. Yang, M. Grätzel, H. Han, *Science* **2014**, *345*, 295.
- [25] L. Chu, S. Zhai, W. Ahmad, J. Zhang, Y. Zang, W. Yan, Y. Li, *Nano Res. Energy* **2022**, *1*, 9120024.
- [26] C. Ran, Y. Wang, W. Gao, Y. Xia, Y. Chen, W. Huang, *Sol. RRL* **2021**, *5*, 2100665.
- [27] J.-X. Song, X.-X. Yin, Z.-F. Li, Y.-W. Li, *Rare Met.* **2021**, *40*, 2730.
- [28] M. Adnan, J. K. Lee, *Sci. Rep.* **2018**, *8*, 2168.
- [29] Z. Li, T. R. Klein, D. H. Kim, M. Yang, J. J. Berry, M. F. A. M. Van Hest, K. Zhu, *Nat. Rev. Mater.* **2018**, *3*, 1.
- [30] S. S. Shin, W. S. Yang, J. H. Noh, J. H. Suk, N. J. Jeon, J. H. Park, J. S. Kim, W. M. Seong, S. I. Seok, *Nat. Commun.* **2015**, *6*, 7410.
- [31] H. Singh, S. Dhakla, P. K. Deendyal, A. Kumar, S. Kumar, M. K. Kashyap, *Indian J. Pure Appl. Phys.* **2023**, *61*, 854.
- [32] M. Liu, M. B. Johnston, H. J. Snaith, *Nature* **2013**, *501*, 395.
- [33] J. Burschka, N. Pellet, S.-J. Moon, R. Humphry-Baker, P. Gao, M. K. Nazeeruddin, M. Grätzel, *Nature* **2013**, *499*, 316.
- [34] Z. Xiao, C. Bi, Y. Shao, Q. Dong, Q. Wang, Y. Yuan, C. Wang, Y. Gao, J. Huang, *Energy Environ. Sci.* **2014**, *7*, 2619.
- [35] Y. Wang, J. Luo, R. Nie, X. Deng, *Energy Technol.* **2016**, *4*, 473.
- [36] B. R. Sutherland, S. Hoogland, M. M. Adachi, P. Kanjanaboos, C. T. O. Wong, J. J. Mcdowell, J. Xu, O. Voznyy, Z. Ning, A. J. Houtepen, E. H. Sargent, *Adv. Mater.* **2015**, *27*, 53.
- [37] R. G. Larson, T. J. Rehg, *Spin Coating, Liquid Film Coating*, Springer, Dordrecht, Netherlands **1997**, pp. 709–734.
- [38] A. Hosseinmardi, A. Moshaii, M. Khodabandeh, Z. Bagheri, S. Abbasian, *J. Mater. Sci.: Mater. Electron.* **2020**, *31*, 16671.

- [39] Q. Jiang, Z. Chu, P. Wang, X. Yang, H. Liu, Y. Wang, Z. Yin, J. Wu, X. Zhang, J. You, *Adv. Mater.* **2017**, *29*, 1703852.
- [40] X. Dai, K. Xu, F. Wei, *Beilstein J. Nanotechnol.* **2020**, *11*, 51.
- [41] M. Yang, Y. Zhou, Y. Zeng, C. Jiang, N. P. Padture, K. Zhu, *Adv. Mater.* **2015**, *27*, 6363.
- [42] W. Chen, Y. Wu, Y. Yue, J. Liu, W. Zhang, X. Yang, H. Chen, E. Bi, I. Ashraful, M. Grätzel, L. Han, *Science* **2015**, *350*, 944.
- [43] S. Obregón, V. Rodríguez-González, *J. Sol-Gel Sci. Technol.* **2022**, *102*, 125.
- [44] L. Huang, C. Li, X. Sun, R. Xu, Y. Du, J. Ni, H. Cai, J. Li, Z. Hu, J. Zhang, *Org. Electron.* **2017**, *40*, 13.
- [45] D. Burkitt, R. Patidar, P. Greenwood, K. Hooper, J. Mcgettrick, S. Dimitrov, M. Colombo, V. Stoichkov, D. Richards, D. Beynon, M. Davies, T. Watson, *Sustainable Energy Fuels* **2020**, *4*, 3340.
- [46] J. Sun, H. Park, Y. Jung, G. Rajbhandari, B. B. Maskey, A. Sapkota, Y. Azuma, Y. Majima, G. Cho, *ACS Omega* **2017**, *2*, 5766.
- [47] R. Abbel, I. De Vries, A. Langen, G. Kirchner, H. T'Mannetje, H. Gorter, J. Wilson, P. Groen, *J. Mater. Res.* **2017**, *32*, 2219.
- [48] A. Sandström, L. Edman, *Energy Technol.* **2015**, *3*, 329.
- [49] F. C. Krebs, N. Espinosa, M. Hösel, R. R. Søndergaard, M. Jørgensen, *Adv. Mater.* **2014**, *26*, 29.
- [50] P. Kaja, K. Ghosh, S. Powar, *Energy, Environment, and Sustainability*, Springer, Singapore **2018**, pp. 341–364.
- [51] M. A. Muhsien, H. H. Hamdan, *Energy Procedia* **2012**, *18*, 300.
- [52] S.-I. Park, Y.-J. Quan, S.-H. Kim, H. Kim, S. Kim, D.-M. Chun, C. S. Lee, M. Taya, W.-S. Chu, S.-H. Ahn, *Int. J. Precis. Eng. Manuf. Green Technol.* **2016**, *3*, 397.
- [53] W. Kohn, L. J. Sham, *Phys. Rev.* **1965**, *140*, A1133.
- [54] P. Hohenberg, W. Kohn, *Phys. Rev.* **1964**, *136*, B864.
- [55] A. Taya, P. Rani, J. Thakur, M. K. Kashyap, *Vacuum* **2019**, *160*, 440.
- [56] A. Taya, S. Kumar, T. A. Hackett, M. K. Kashyap, *Vacuum* **2022**, *201*, 111106.
- [57] R. J. Bartlett, *Annu. Rev. Phys. Chem.* **1981**, *32*, 359.
- [58] M. S. Hybertsen, S. G. Louie, *Phys. Rev. B* **1986**, *34*, 5390.
- [59] E. Runge, E. K. U. Gross, *Phys. Rev. Lett.* **1984**, *52*, 997.
- [60] D. M. Ceperley, B. J. Alder, *Phys. Rev. Lett.* **1980**, *45*, 566.
- [61] R. Car, M. Parrinello, *Phys. Rev. Lett.* **1985**, *55*, 2471.
- [62] M. Elstner, D. Porezag, G. Jungnickel, J. Elsner, M. Haugk, T. Frauenheim, S. Suhai, G. Seifert, *Phys. Rev. B* **1998**, *58*, 7260.
- [63] M. J. S. Dewar, E. G. Zoebisch, E. F. Healy, J. J. P. Stewart, *J. Am. Chem. Soc.* **1985**, *107*, 3902.
- [64] K. T. Schütt, F. Arbabzadah, S. Chmiela, K. R. Müller, A. Tkatchenko, *Nat. Commun.* **2017**, *8*, 13890.
- [65] P. Raccuglia, K. C. Elbert, P. D. F. Adler, C. Falk, M. B. Wenny, A. Mollo, M. Zeller, S. A. Friedler, J. Schrier, A. J. Norquist, *Nature* **2016**, *533*, 73.
- [66] N.-G. Park, K. Zhu, *Nat. Rev. Mater.* **2020**, *5*, 333.
- [67] P. K. Deendyal, S. Dhakla, H. Singh, A. Taya, S. Kumar, M. K. Kashyap, *ChemistrySelect* **2023**, *8*, e202302252.
- [68] H. Singh, S. Dhakla, P. K. Deendyal, A. Kumar, S. Kumar, M. K. Kashyap, *Appl. Res.* **2023**, *2*, e202200077.
- [69] S. Dhakla, P. K. Deendyal, H. Singh, M. Mishra, S. Kumar, M. K. Kashyap, *Indian J. Pure Appl. Phys.* **2023**, *61*, 851.
- [70] P. K. Deendyal, S. Dhakla, H. Singh, S. Kumar, M. K. Kashyap, *Indian J. Pure Appl. Phys.* **2023**, *61*, 931.
- [71] S. Dhakla, P. K. Deendyal, H. Singh, S. Kumar, M. K. Kashyap, *IEEE J. Photovoltaics* **2024**, *14*, 85.
- [72] A. Husainat, W. Ali, P. Cofe, J. Attia, J. Fuller, *Am. J. Opt. Photonics* **2019**, *7*, 33.
- [73] S. S. Nishat, M. J. Hossain, F. E. Mullick, A. Kabir, S. Chowdhury, S. Islam, M. Hossain, *J. Phys. Chem. C* **2021**, *125*, 13158.
- [74] J. Laali, A. Hamedani, G. Alahyarizadeh, A. Minucheer, *Superlattices Microstruct.* **2020**, *143*, 106551.
- [75] M. Lekshmi, S. Saroon, A. Albert, C. O. Sreekala, *Mater. Today Proc.* **2021**, *46*, 3114.
- [76] Q. An, F. Paulus, D. Becker-Koch, C. Cho, Q. Sun, A. Weu, S. Bitton, N. Tessler, Y. Vaynzof, *Matter* **2021**, *4*, 1683.
- [77] F. A. Stevie, C. L. Donley, *J. Vac. Sci. Technol., A* **2020**, *38*, 063204.
- [78] E. L. Meyer, J. C. Nwodo, *Appl. Sci.* **2020**, *10*, 4534.
- [79] Q. Sun, P. Fassel, D. Becker-Koch, A. Bausch, B. Rivkin, S. Bai, P. E. Hopkinson, H. J. Snaith, Y. Vaynzof, *Adv. Energy Mater.* **2017**, *7*, 1700977.
- [80] F. Matsumoto, S. M. Vorpahl, J. Q. Banks, E. Sengupta, D. S. Ginger, *J. Phys. Chem. C* **2015**, *119*, 20810.
- [81] Y. Wei, P. Audebert, L. Galmiche, J.-S. Laurent, E. Deleporte, *Materials* **2014**, *7*, 4789.
- [82] J. Wei, Q. Wang, J. Huo, F. Gao, Z. Gan, Q. Zhao, H. Li, *Adv. Energy Mater.* **2021**, *11*, 2002326.
- [83] B. Park, S. I. Seok, *Adv. Mater.* **2019**, *31*, 1805337.
- [84] G. Han, H. D. Hadi, A. Bruno, S. A. Kulkarni, T. M. Koh, L. H. Wong, C. Soci, N. Mathews, S. Zhang, S. G. Mhaisalkar, *J. Phys. Chem. C* **2018**, *122*, 13884.
- [85] J. H. Noh, S. H. Im, J. H. Heo, T. N. Mandal, S. Il Seok, *Nano Lett.* **2013**, *13*, 1764.
- [86] B. Suarez, V. Gonzalez-Pedro, T. S. Ripolles, R. S. Sanchez, L. Otero, I. Mora-Sero, *J. Phys. Chem. Lett.* **2014**, *5*, 1628.
- [87] Q. Tai, P. You, H. Sang, Z. Liu, C. Hu, H. L. W. Chan, F. Yan, *Nat. Commun.* **2016**, *7*, 11110.
- [88] S. Ameen, M. A. Rub, S. A. Kosa, K. A. Alamry, M. S. Akhtar, H. Shin, H. Seo, A. M. Asiri, M. K. Nazeeruddin, *ChemSusChem* **2016**, *9*, 10.
- [89] A. Abate, T. Leijtens, S. Pathak, J. Teuscher, R. Avolio, M. E. Errico, J. Kirkpatrick, J. M. Ball, P. Docampo, I. Mcpherson, H. J. Snaith, *Phys. Chem. Chem. Phys.* **2013**, *15*, 2572.
- [90] C. Huang, W. Fu, C.-Z. Li, Z. Zhang, W. Qiu, M. Shi, P. Heremans, A. K.-Y. Jen, H. Chen, *J. Am. Chem. Soc.* **2016**, *138*, 2528.
- [91] J. H. Heo, S. H. Im, J. H. Noh, T. N. Mandal, C.-S. Lim, J. A. Chang, Y. H. Lee, H. Kim, A. Sarkar, M. K. Nazeeruddin, M. Grätzel, S. I. Seok, *Nat. Photonics* **2013**, *7*, 486.
- [92] Q. Zhao, R. Wu, Z. Zhang, J. Xiong, Z. He, B. Fan, Z. Dai, B. Yang, X. Xue, P. Cai, S. Zhan, X. Zhang, J. Zhang, *Org. Electron.* **2019**, *71*, 106.
- [93] J. You, L. Meng, T.-B. Song, T.-F. Guo, Y. Yang, W.-H. Chang, Z. Hong, H. Chen, H. Zhou, Q. Chen, Y. Liu, N. De Marco, Y. Yang, *Nat. Nanotechnol.* **2016**, *11*, 75.
- [94] N. J. Jeon, H. G. Lee, Y. C. Kim, J. Seo, J. H. Noh, J. Lee, S. Il Seok, *J. Am. Chem. Soc.* **2014**, *136*, 7837.
- [95] X. Dong, H. Hu, B. Lin, J. Ding, N. Yuan, *Chem. Commun.* **2014**, *50*, 14405.
- [96] S. S. Shin, E. J. Yeom, W. S. Yang, S. Hur, M. G. Kim, J. Im, J. Seo, J. H. Noh, S. Il Seok, *Science* **2017**, *356*, 167.
- [97] T. Hu, T. Becker, N. Pourdavoud, J. Zhao, K. O. Brinkmann, R. Heiderhoff, T. Gahlmann, Z. Huang, S. Olthof, K. Meerholz, D. Többsen, B. Cheng, Y. Chen, T. Riedl, *Adv. Mater.* **2017**, *29*, 1606656.
- [98] J. P. Correa Baena, L. Steier, W. Tress, M. Saliba, S. Neutzner, T. Matsui, F. Giordano, T. J. Jacobsson, A. R. Srimath Kandada, S. M. Zakeeruddin, A. Petrozza, A. Abate, M. K. Nazeeruddin, M. Grätzel, A. Hagfeldt, *Energy Environ. Sci.* **2015**, *8*, 2928.
- [99] Q. Jiang, L. Zhang, H. Wang, X. Yang, J. Meng, H. Liu, Z. Yin, J. Wu, X. Zhang, J. You, *Nat. Energy* **2017**, *2*, 1.
- [100] S. S. Mali, C. Su Shim, C. Kook Hong, *Sci. Rep.* **2015**, *5*, 11424.
- [101] L. Wang, W. Fu, Z. Gu, C. Fan, X. Yang, H. Li, H. Chen, *J. Mater. Chem. C* **2014**, *2*, 9087.
- [102] R. Singh, A. Giri, M. Pal, K. Thiyagarajan, J. Kwak, J.-J. Lee, U. Jeong, K. Cho, *J. Mater. Chem. A* **2019**, *7*, 7151.

- [103] A. Gheno, T. T. Thu Pham, C. Di Bin, J. Bouclé, B. Ratier, S. Vedraïne, *Sol. Energy Mater. Sol. Cells* **2017**, *161*, 347.
- [104] A. Priyadarshi, A. Bashir, J. T. Gunawan, L. J. Haur, A. Bruno, Z. Akhter, N. Mathews, S. G. Mhaisalkar, *Energy Technol.* **2017**, *5*, 1866.
- [105] Y. Rong, Z. Tang, Y. Zhao, X. Zhong, S. Venkatesan, H. Graham, M. Patton, Y. Jing, A. M. Guloy, Y. Yao, *Nanoscale* **2015**, *7*, 10595.
- [106] M. Xiao, F. Huang, W. Huang, Y. Dkhissi, Y. Zhu, J. Etheridge, A. Gray-Weale, U. Bach, Y. Cheng, L. Spiccia, *Angew. Chem., Int. Ed.* **2014**, *53*, 9898.
- [107] X. Fang, Y. Wu, Y. Lu, Y. Sun, S. Zhang, J. Zhang, W. Zhang, N. Yuan, J. Ding, *J. Mater. Chem. C* **2017**, *5*, 842.
- [108] Y. Guo, K. Shoyama, W. Sato, E. Nakamura, *Adv. Energy Mater.* **2016**, *6*, 1502317.
- [109] D. Bi, P. Gao, R. Scopelliti, E. Oveisi, J. Luo, M. Grätzel, A. Hagfeldt, M. K. Nazeeruddin, *Adv. Mater.* **2016**, *28*, 2910.
- [110] J. Pan, C. Mu, Q. Li, W. Li, D. Ma, D. Xu, *Adv. Mater.* **2016**, *28*, 8309.
- [111] F. Bella, G. Griffini, J.-P. Correa-Baena, G. Saracco, M. Grätzel, A. Hagfeldt, S. Turri, C. Gerbaldi, *Science* **2016**, *354*, 203.
- [112] Y. Liu, S. Akin, L. Pan, R. Uchida, N. Arora, J. V. Milić, A. Hinderhofer, F. Schreiber, A. R. Uhl, S. M. Zakeeruddin, A. Hagfeldt, M. Ibrahim Dar, M. Grätzel, *Sci. Adv.* **2019**, *5*, eaaw2543.
- [113] G. Niu, W. Li, F. Meng, L. Wang, H. Dong, Y. Qiu, *J. Mater. Chem. A* **2014**, *2*, 705.
- [114] V. D'Innocenzo, G. Grancini, M. J. P. Alcocer, A. R. S. Kandada, S. D. Stranks, M. M. Lee, G. Lanzani, H. J. Snaith, A. Petrozza, *Nat. Commun.* **2014**, *5*, 3586.
- [115] J. Lee, D. Seol, A. Cho, N. Park, *Adv. Mater.* **2014**, *26*, 4991.
- [116] A. Amat, E. Mosconi, E. Ronca, C. Quarti, P. Umari, M. K. Nazeeruddin, M. Grätzel, F. De Angelis, *Nano Lett.* **2014**, *14*, 3608.
- [117] J. Lee, D. Kim, H. Kim, S. Seo, S. M. Cho, N. Park, *Adv. Energy Mater.* **2015**, *5*, 1501310.
- [118] M. R. Leyden, M. V. Lee, S. R. Raga, Y. Qi, *J. Mater. Chem. A* **2015**, *3*, 16097.
- [119] F. Wang, W. Geng, Y. Zhou, H. Fang, C. Tong, M. A. Loi, L. Liu, N. Zhao, *Adv. Mater.* **2016**, *28*, 9986.
- [120] R. Cheacharoen, N. Rolston, D. Harwood, K. A. Bush, R. H. Dauskardt, M. D. McGehee, *Energy Environ. Sci.* **2018**, *11*, 144.
- [121] T. Liu, Y. Zhou, Z. Li, L. Zhang, M. Ju, D. Luo, Y. Yang, M. Yang, D. H. Kim, W. Yang, N. P. Padture, M. C. Beard, X. C. Zeng, K. Zhu, Q. Gong, R. Zhu, *Adv. Energy Mater.* **2018**, *8*, 1800232.
- [122] N. J. Jeon, H. Na, E. H. Jung, T.-Y. Yang, Y. G. Lee, G. Kim, H.-W. Shin, S. Il Seok, J. Lee, J. Seo, *Nat. Energy* **2018**, *3*, 682.
- [123] Y. H. Lin, N. Sakai, P. Da, J. Wu, H. C. Sansom, A. J. Ramadan, S. Mahesh, J. Liu, R. D. Oliver, J. Lim, L. Aspirtarte, *Science* **2020**, *369*, 96.
- [124] J. Xue, R. Wang, X. Chen, C. Yao, X. Jin, K.-L. Wang, W. Huang, T. Huang, Y. Zhao, Y. Zhai, D. Meng, S. Tan, R. Liu, Z.-K. Wang, C. Zhu, K. Zhu, M. C. Beard, Y. Yan, Y. Yang, *Science* **2021**, *371*, 636.
- [125] J. A. Christians, P. Schulz, J. S. Tinkham, T. H. Schloemer, S. P. Harvey, B. J. Tremolet De Villers, A. Sellinger, J. J. Berry, J. M. Luther, *Nat. Energy* **2018**, *3*, 68.
- [126] Z. Dai, S. K. Yadavalli, M. Chen, A. Abbaspourtamijani, Y. Qi, N. P. Padture, *Science* **2021**, *372*, 618.
- [127] Q. Jiang, Y. Zhao, X. Zhang, X. Yang, Y. Chen, Z. Chu, Q. Ye, X. Li, Z. Yin, J. You, *Nat. Photonics* **2019**, *13*, 460.
- [128] E. H. Jung, N. J. Jeon, E. Y. Park, C. S. Moon, T. J. Shin, T.-Y. Yang, J. H. Noh, J. Seo, *Nature* **2019**, *567*, 511.
- [129] R. Azmi, N. Nurrosyid, S.-H. Lee, M. Al Mubarak, W. Lee, S. Hwang, W. Yin, T. K. Ahn, T.-W. Kim, D. Y. Ryu, Y. R. Do, S.-Y. Jang, *ACS Energy Lett.* **2020**, *5*, 1396.
- [130] H. Min, D. Y. Lee, J. Kim, G. Kim, K. S. Lee, J. Kim, M. J. Paik, Y. K. Kim, K. S. Kim, M. G. Kim, T. J. Shin, S. Il Seok, *Nature* **2021**, *598*, 444.
- [131] G. Giorgi, J. I. Fujisawa, H. Segawa, K. Yamashita, *J. Phys. Chem. C* **2015**, *119*, 4694.
- [132] N. De Marco, H. Zhou, Q. Chen, P. Sun, Z. Liu, L. Meng, E.-P. Yao, Y. Liu, A. Schiffer, Y. Yang, *Nano Lett.* **2016**, *16*, 1009.
- [133] A. D. Jodlowski, C. Roldán-Carmona, G. Grancini, M. Salado, M. Ralairisoa, S. Ahmad, N. Koch, L. Camacho, G. De Miguel, M. K. Nazeeruddin, *Nat. Energy* **2017**, *2*, 972.
- [134] L. Gao, X. Li, Y. Liu, J. Fang, S. Huang, I. Spanopoulos, X. Li, Y. Wang, L. Chen, G. Yang, M. G. Kanatzidis, *ACS Appl. Mater. Interfaces* **2020**, *12*, 43885.
- [135] Z. Li, L. Hao, D. Liu, X. Sun, Q. Zhao, Z. Shao, C. Chen, X. Wang, L. Wang, G. Cui, S. Pang, *Sol. RRL* **2022**, *6*, 2200003.
- [136] Y. Ma, L. Zhang, Y. Xu, R. Hu, W. Liu, M. Du, L. Chu, J. Zhang, X. Li, R. Xia, W. Huang, *ACS Appl. Mater. Interfaces* **2022**, *14*, 11200.
- [137] W. Zhang, J. Xiong, J. Li, W. A. Daoud, *J. Mater. Chem. A* **2019**, *7*, 9486.
- [138] S. Mazumdar, Y. Zhao, X. Zhang, *Front. Electron.* **2021**, *2*, 712785.
- [139] T. A. Chowdhury, M. A. Bin Zafar, M. Sajjad-Ul Islam, M. Shahinuzzaman, M. A. Islam, M. U. Khandaker, *RSC Adv.* **2023**, *13*, 1787.
- [140] Q.-Q. Chu, Z. Sun, D. Wang, B. Cheng, H. Wang, C.-P. Wong, B. Fang, *Matter* **2023**, *6*, 3838.
- [141] D. Zhang, D. Li, Y. Hu, A. Mei, H. Han, *Commun. Mater.* **2022**, *3*, 58.
- [142] K. Lochhead, E. Johlin, D. Yang, K. Lochhead, E. Johlin, D. Yang, *Thin Films - Deposition Methods and Applications*, IntechOpen **2022**, <https://doi.org/10.5772/INTECHOPEN.107189>.
- [143] S. F. Ahmed, N. Islam, P. S. Kumar, A. T. Hoang, M. Mofijur, A. Inayat, G. M. Shafiqullah, D.-V. N. Vo, I. A. Badruddin, S. Kamangar, *Mater. Today Chem.* **2023**, *27*, 101284.
- [144] Y. Zhao, W. Zhou, Z. Han, D. Yu, Q. Zhao, *Phys. Chem. Chem. Phys.* **2021**, *23*, 94.
- [145] J. Zhuang, J. Wang, F. Yan, *Nano-Micro Lett.* **2023**, *15*, 84.
- [146] A. Kumar, S. Singh, A. Sharma, E. M. Ahmed, *Opt. Mater.* **2022**, *132*, 112846.
- [147] T. Dai, Q. Cao, L. Yang, M. Aldamasy, M. Li, Q. Liang, H. Lu, Y. Dong, Y. Yang, *Crystals* **2021**, *11*, 295.
- [148] Y. Chen, T. Chen, L. Dai, *Adv. Mater.* **2015**, *27*, 1053.
- [149] Y. Chen, B. Li, W. Huang, D. Gao, Z. Liang, *Chem. Commun.* **2015**, *51*, 11997.
- [150] H.-L. Hsu, C.-C. Chang, C.-P. Chen, B.-H. Jjiang, R.-J. Jeng, C.-H. Cheng, *J. Mater. Chem. A* **2015**, *3*, 9271.
- [151] X. Li, M. Ibrahim Dar, C. Yi, J. Luo, M. Tschumi, S. M. Zakeeruddin, M. K. Nazeeruddin, H. Han, M. Grätzel, *Nat. Chem.* **2015**, *7*, 703.
- [152] C.-H. Chiang, C.-G. Wu, *Nat. Photonics* **2016**, *10*, 196.
- [153] Y. Zhao, J. Wei, H. Li, Y. Yan, W. Zhou, D. Yu, Q. Zhao, *Nat. Commun.* **2016**, *7*, 10228.
- [154] Q. Wang, Q. Dong, T. Li, A. Gruverman, J. Huang, *Adv. Mater.* **2016**, *28*, 6734.
- [155] Y. Wu, F. Xie, H. Chen, X. Yang, H. Su, M. Cai, Z. Zhou, T. Noda, L. Han, *Adv. Mater.* **2017**, *29*, 1701073.
- [156] X. Wan, Y. Jiang, Z. Qiu, H. Zhang, X. Zhu, I. Sikandar, X. Liu, X. Chen, B. Cao, *ACS Appl. Energy Mater.* **2018**, *1*, 3947.
- [157] M. Jung, T. J. Shin, J. Seo, G. Kim, S. I. Seok, *Energy Environ. Sci.* **2018**, *11*, 2188.
- [158] Y. Lin, Y. Bai, Y. Fang, Z. Chen, S. Yang, X. Zheng, S. Tang, Y. Liu, J. Zhao, J. Huang, *J. Phys. Chem. Lett.* **2018**, *9*, 654.
- [159] H. Zhang, X. Ren, X. Chen, J. Mao, J. Cheng, Y. Zhao, Y. Liu, J. Milic, W.-J. Yin, M. Grätzel, W. C. H. Choy, *Energy Environ. Sci.* **2018**, *11*, 2253.

- [160] M. B. Islam, M. Yanagida, Y. Shirai, Y. Nabetani, K. Miyano, *Sol. Energy Mater. Sol. Cells* **2019**, *195*, 323.
- [161] J. Yang, S. Xiong, T. Qu, Y. Zhang, X. He, X. Guo, Q. Zhao, S. Braun, J. Chen, J. Xu, Y. Li, X. Liu, C. Duan, J. Tang, M. Fahlman, Q. Bao, *ACS Appl. Mater. Interfaces* **2019**, *11*, 13491.
- [162] R. Wang, J. Xue, L. Meng, J.-W. Lee, Z. Zhao, P. Sun, L. Cai, T. Huang, Z. Wang, Z.-K. Wang, Y. Duan, J. L. Yang, S. Tan, Y. Yuan, Y. Huang, Y. Yang, *Joule* **2019**, *3*, 1464.
- [163] C. Li, J. Yin, R. Chen, X. Lv, X. Feng, Y. Wu, J. Cao, *J. Am. Chem. Soc.* **2019**, *141*, 6345.
- [164] Y. Qiang, Y. Xie, Y. Qi, P. Wei, H. Shi, C. Geng, H. Liu, *Sol. Energy* **2020**, *201*, 523.
- [165] B. Taheri, E. Calabrò, F. Matteocci, D. Di Girolamo, G. Cardone, A. Liscio, A. Di Carlo, F. Brunetti, *Energy Technol.* **2020**, *8*, 1901284.
- [166] H. Wang, Y. Zhao, Z. Wang, Y. Liu, Z. Zhao, G. Xu, T.-H. Han, J.-W. Lee, C. Chen, D. Bao, Y. Huang, Y. Duan, Y. Yang, *Nano Energy* **2020**, *69*, 104375.
- [167] H.-C. Chen, J.-M. Lan, H.-L. Hsu, C.-W. Li, T.-S. Shieh, K.-T. Wong, C.-P. Chen, *Mater. Chem. Front.* **2021**, *5*, 3378.
- [168] J. Tao, Z. Wang, H. Wang, J. Shen, X. Liu, J. Xue, H. Guo, G. Fu, W. Kong, S. Yang, *ACS Appl. Mater. Interfaces* **2021**, *13*, 44451.
- [169] X. Li, J. Du, H. Duan, H. Wang, L. Fan, Y. Sun, Y. Sui, J. Yang, F. Wang, L. Yang, *Nano Res.* **2022**, *15*, 1375.
- [170] C. Duan, J. Dai, *Opt. Express* **2022**, *30*, 38104.
- [171] S. Liu, D. Zhang, Y. Sheng, W. Zhang, Z. Qin, M. Qin, S. Li, Y. Wang, C. Gao, Q. Wang, Y. Ming, C. Liu, K. Yang, Q. Huang, J. Qi, Q. Gao, K. Chen, Y. Hu, Y. Rong, X. Lu, A. Mei, H. Han, *Fundam. Res.* **2022**, *2*, 276.
- [172] P. Zhou, S. Lu, Y. Mo, J. Cheng, C. Jiao, X.-L. Zhang, W. Li, G. Liang, J. Wang, F. Huang, Y.-B. Cheng, *Sol. RRL* **2023**, *7*, 2201067.
- [173] M. Bag, L. A. Renna, R. Y. Adhikari, S. Karak, F. Liu, P. M. Lahti, T. P. Russell, M. T. Tuominen, D. Venkataraman, *J. Am. Chem. Soc.* **2015**, *137*, 13130.
- [174] S. Yang, W. Liu, L. Zuo, X. Zhang, T. Ye, J. Chen, C.-Z. Li, G. Wu, H. Chen, *J. Mater. Chem. A* **2016**, *4*, 9430.
- [175] T. Y. Wen, S. Yang, P. F. Liu, L. J. Tang, H. W. Qiao, X. Chen, X. H. Yang, Y. Hou, H. G. Yang, *Adv. Energy Mater.* **2018**, *8*, 1703143.
- [176] M. Kim, S. G. Motti, R. Sorrentino, A. Petrozza, *Energy Environ. Sci.* **2018**, *11*, 2609.
- [177] R. Checharoen, C. C. Boyd, G. F. Burkhard, T. Leijtens, J. A. Raiford, K. A. Bush, S. F. Bent, M. D. McGehee, *Sustainable Energy Fuels* **2018**, *2*, 2398.
- [178] J. Kim, A. J. Yun, B. Gil, Y. Lee, B. Park, *Adv. Funct. Mater.* **2019**, *29*, 1905190.
- [179] X. Zheng, Y. Hou, C. Bao, J. Yin, F. Yuan, Z. Huang, K. Song, J. Liu, J. Troughton, N. Gasparini, C. Zhou, Y. Lin, D.-J. Xue, B. Chen, A. K. Johnston, N. Wei, M. N. Hedhili, M. Wei, A. Y. Alsalloum, P. Maity, B. Turedi, C. Yang, D. Baran, T. D. Anthopoulos, Y. Han, Z.-H. Lu, O. F. Mohammed, F. Gao, E. H. Sargent, O. M. Bakr, *Nat. Energy* **2020**, *5*, 131.
- [180] M. Jeong, I. W. Choi, E. M. Go, Y. Cho, M. Kim, B. Lee, S. Jeong, Y. Jo, H. W. Choi, J. Lee, J. H. Bae, S. K. Kwak, D. S. Kim, C. Yang, *Science* **2020**, *369*, https://doi.org/10.1126/SCIENCE.ABB7167/SUPPL_FILE/ABB7167_JEONG_SM.PDF.
- [181] S. Wu, Z. Li, M.-Q. Li, Y. Diao, F. Lin, T. Liu, J. Zhang, P. Tieu, W. Gao, F. Qi, X. Pan, Z. Xu, Z. Zhu, A. K.-Y. Jen, *Nat. Nanotechnol.* **2020**, *15*, 934.
- [182] L. Shi, M. P. Bucknall, T. L. Young, M. Zhang, L. Hu, J. Bing, D. S. Lee, J. Kim, T. Wu, N. Takamure, D. R. McKenzie, S. Huang, M. A. Green, A. W. Y. Ho-Baillie, *Science* **2020**, *368*, eaba2412.
- [183] L. Qiu, S. He, Z. Liu, L. K. Ono, D.-Y. Son, Y. Liu, G. Tong, Y. Qi, *J. Mater. Chem. A* **2020**, *8*, 23404.
- [184] L. Gil-Escrig, C. Dreessen, I. C. Kaya, B. S. Kim, F. Palazon, M. Sessolo, H. J. Bolink, *ACS Energy Lett.* **2020**, *5*, 3053.
- [185] Z. Li, P. Li, G. Chen, Y. Cheng, X. Pi, X. Yu, D. Yang, L. Han, Y. Zhang, Y. Song, *ACS Appl. Mater. Interfaces* **2020**, *12*, 39082.
- [186] R. Chen, S. Liu, X. Xu, F. Ren, J. Zhou, X. Tian, Z. Yang, X. Guanz, Z. Liu, S. Zhang, Y. Zhang, Y. Wu, L. Han, Y. Qi, W. Chen, *Energy Environ. Sci.* **2022**, *15*, 2567.
- [187] S. Wang, L. Tan, J. Zhou, M. Li, X. Zhao, H. Li, W. Tress, L. Ding, M. Graetzel, C. Yi, *Joule* **2022**, *6*, 1344.
- [188] J. Suo, B. Yang, J. Jeong, T. Zhang, S. Olthof, F. Gao, M. Grätzel, G. Boschloo, A. Hagfeldt, *Nano Energy* **2022**, *94*, 106924.
- [189] S. Zhan, Y. Duan, Z. Liu, L. Yang, K. He, Y. Che, W. Zhao, Y. Han, S. Yang, G. Zhao, N. Yuan, J. Ding, S. Liu, *Adv. Energy Mater.* **2022**, *12*, 2200867.
- [190] J. Sun, Y. Gu, Y. Lu, J. Hu, T. Chen, C. Zhu, P. Luo, *Chem. Eng. J.* **2023**, *468*, 143722.
- [191] T. Pan, W. Zhou, Q. Wei, Z. Peng, H. Wang, X. Jiang, Z. Zang, H. Li, D. Yu, Q. Zhou, M. Pan, W. Zhou, Z. Ning, *Adv. Mater.* **2023**, *35*, 2208522.
- [192] Z. Li, M. Wu, L. Yang, K. Guo, Y. Duan, Y. Li, K. He, Y. Xing, Z. Zhang, H. Zhou, D. Xu, J. Wang, H. Zou, D. Li, Z. Liu, *Adv. Funct. Mater.* **2023**, *33*, 2212606.
- [193] K. Poorkazem, T. Kelly, *Sustainable Energy Fuels* **2018**, *2*, 1332.
- [194] N. Cheng, W. Li, M. Zhang, H. Wu, S. Sun, Z. Zhao, Z. Xiao, Z. Sun, W. Zi, L. Fang, *Curr. Appl. Phys.* **2019**, *19*, 25.
- [195] Y. Zhou, H. Xue, Y. Jia, G. Brocks, S. Tao, N. Zhao, *Adv. Funct. Mater.* **2019**, *29*, 1905739.
- [196] S. Ramos-Terrón, J. F. Illanes, D. Bohoyo-Gil, L. Camacho, G. De Miguel, *Sol. RRL* **2021**, *5*, 2100586.
- [197] H. Dong, S. Pang, F. He, H. Yang, W. Zhu, D. Chen, H. Xi, J. Zhang, Y. Hao, C. Zhang, *Sol. RRL* **2021**, *5*, 2100097.
- [198] B. Huang, X. Xia, X. Wang, F. Li, *Sol. Energy Mater. Sol. Cells* **2022**, *240*, 111682.
- [199] M. Balaji Gandhi, A. Valluvar Oli, S. Nicholson, M. Adelt, R. Martin, Y. Chen, M. Babu Sridharan, A. Ivaturi, *Sol. Energy* **2023**, *253*, 1.



Parvesh K. Deendyal is working as a Lecturer at Govt. Polytechnic for Women, Faridabad, Haryana, India since March 2023. He has been working as a Ph.D. scholar under the supervision of Prof. Manish K. Kashyap at Renewable Energy Laboratory, School of Physical Sciences, Jawaharlal Nehru University, New Delhi, India since 2021. He completed his M.Sc. from Kurukshetra University, Kurukshetra, Haryana, India in 2020. His areas of research interest are Theoretical Condensed Matter Physics and Materials Science with a main emphasis on device fabrication and numerical simulations of HHP Solar Cells.



Shweta Dhakla completed her M.Sc. from Kurukshetra University, Kurukshetra, Haryana, India in 2020. She has been working as Ph.D. scholar under the supervision of Prof. Manish K. Kashyap at Renewable Energy Laboratory, School of Physical Sciences, Jawaharlal Nehru University, New Delhi, India since 2021. Her areas of research interest are Theoretical Condensed Matter Physics and Materials Science with a main emphasis on device fabrication and numerical simulations of HHP Solar Cells.



Ankur Taya is working as an assistant professor at Mukand Lal National College, Yamuna Nagar, Haryana, India since 2019. She earned her Ph.D. degree in Physics from Kurukshetra University, Kurukshetra (Haryana) India under the guidance of Prof. Manish K. Kashyap in 2022. With a teaching experience of 4.5 years, she is actively involved in various research endeavors. Her areas of research interests included Theoretical Condensed Matter Physics, Materials Science with a main emphasis on DFT and ML based studies of HHP solar cells.



Renu Singla has been working as an assistant professor in Department of Physics, Daulat Ram College, University of Delhi since 2022. She earned her Ph.D. degree in Physics from Kurukshetra University, Kurukshetra (Haryana) India under the guidance of Prof. Manish K. Kashyap in 2022. Her area of research interest is Theoretical Condensed Matter Physics with a main emphasis on DFT simulations of permanent magnet materials, 2D materials and van der heterostructures, and HHP materials of PV.



Harpreet Singh is currently doing his Ph.D. at Department of Physics, Institute of Integrated and Honors Studies, Kurukshetra University, Kurukshetra since 2019 under the supervision of Dr. Anand Kumar (IHS, KUK) and Prof. Manish K. Kashyap (JNU, New Delhi). He completed M.Sc. from Kurukshetra University, Kurukshetra, Haryana, India in 2019. His current area of interest is Material Science with a main emphasis on HHP solar cells, Thin Film synthesis and characterizations, and Device Simulation using SCAPS-1D.



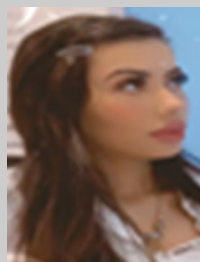
Sarvesh Kumar is working as Scientist-E at Inter-University Accelerator Centre, New Delhi, India since 2005. He earned his Ph.D. degree from Jawaharlal Nehru University, New Delhi, India. His areas of research interests are Materials Science, Plasma Physics, and Accelerator Physics with a main emphasis on HHP solar cells, plasma instabilities in ECR ion sources, interaction of heavy ion with plasma, and novel acceleration schemes of charged particles in accelerators.



Timothy A. Hackett has been contributing to Charles River Laboratories in Ashland, Ohio, as a Research Scientist since 2023. He has obtained his Ph.D. degree from University of Nebraska - Lincoln in Lincoln, Nebraska, United States. With 7 years of combined teaching and research expertise, his focus spans Material Sciences, Chemical and Biomolecular Engineering, Theoretical Condensed Matter Physics, and Materials Science.



Manish K. Kashyap has been working as a professor at School of Physical Sciences, Jawaharlal Nehru University, New Delhi, India since 2020. He has a rich teaching experience of 17 years to UG/PG students. He has supervised 8 Ph.D. students and 1 post-doctoral fellow till date and 6 Ph.D. students are still working under his guidance. His areas of research interests are Theoretical Condensed Matter Physics, Materials Science, Plasma Physics, Accelerator Physics with a main emphasis on HHP solar cells, 2D materials/van der Waals' heterostructures, DMS and Heusler Alloys for Spintronics and Plasma instabilities in ECR ion sources.



Dania Ali is working as assistant at Charles University, Czech Republic. Her areas of research interests are Medical, Medicine, Surgery, Biophysics, Nanotechnology, Nanotechnology in medicine, MRI, Theoretical Condensed Matter Physics, Interface, Materials Science, Plasma Physics, Accelerator Physics with a main emphasis on HHP solar cells, 2D materials, Optical properties, Laser and Nonlinear optical properties.



Ali H. Reshak (H-index WoS = 50, Scopus = 51 and 56 at Google Scholar, with more than 15 000 citations) is a full professor at University of Basrah, Iraq, the Vice Chancellor of Basrah University. Also as a senior fellow full professor at Czech Technical University –Prague– Czech Republic, and full professor and Principal Research Fellow at University Malaysia Perlis, Malaysia. Prof. Reshak is the winner of the Abdul Hameed Shoman Award. He is a Durham University senior fellow (UK) and Malaya University Principal Research fellow (Malaysia). Recently Prof. Dr. Eng. Ali H. Reshak was awarded an Honorary Doctorate of Engineering from the University of Malaysia Perlis for his achievements in Sciences and Technology.